High-throughput phenotyping of infection by diverse microsporidia species reveals a wild *C. elegans* strain with opposing resistance and susceptibility traits

Calvin Mok[1#], Meng A. Xiao[1*], Yin C. Wan[1*], Winnie Zhao[1], Shanzeh M. Ahmed[1], Robert J. Luallen[2] and Aaron W. Reinke[1#]

[1] Department of Molecular Genetics, University of Toronto, Toronto, ON, Canada

[2] Department of Biology, San Diego State University, San Diego, CA 92182, USA

*These authors contributed equally

#Corresponding authors

calvin.mok@utoronto.ca

aaron.reinke@utoronto.ca

Abstract

Animals are under constant selective pressure from a myriad of diverse pathogens. Microsporidia are ubiquitous animal parasites, but the influence they exert on shaping animal genomes is mostly unknown. Using multiplexed competition assays, we measured the impact of four different species of microsporidia on 22 wild isolates of *Caenorhabditis elegans*. This resulted in the identification and confirmation of 13 strains with significantly altered population fitness profiles under infection conditions. One of these identified strains, JU1400, is sensitive to an epidermal-infecting species by lacking tolerance to infection. JU1400 is also resistant to an intestinal-infecting species and can specifically recognize and destroy this pathogen. Genetic mapping of JU1400 demonstrates

that these two opposing phenotypes are caused by separate loci. Transcriptional analysis reveals the JU1400 sensitivity to epidermal microsporidia infection results in a response pattern that shares similarity to toxin-induced responses. In contrast, we do not observe JU1400 intestinal resistance being regulated at the transcriptional level. The transcriptional response to these four microsporidia species is conserved, with *C. elegans* strain-specific differences in potential immune genes. Together, our results show that phenotypic differences to microsporidia infection amongst *C. elegans* are common and that animals can evolve species-specific genetic interactions.

Introduction

Obligate intracellular parasites only propagate inside of host cells, which places extreme pressure on the host, resulting in genomic changes [1–3]. Animals have coevolved with pathogens and genetic variation to pathogen susceptibility is common in animal populations [4,5]. Much of this genetic and phenotypic diversity to infection is specific to individual species of pathogens or even to different strains [6,7]. Hosts can evolve several ways to improve their fitness in the presence of pathogens. They can become more resistant by preventing pathogen invasion or by limiting pathogen growth [8]. Alternatively, hosts can evolve to better tolerate the infection, by limiting the negative effects of infection without reducing the amount of pathogen [9,10].

Microsporidia are a large phylum of eukaryotic obligate intracellular pathogens with a wide host range including humans and agriculturally important animals such as honey bees and shrimp [11–14]. Microsporidia infections cause developmental delays, a reduction in progeny, and increased mortality [15–17]. Several studies have shown that microsporidia can affect host population dynamics and evolution. Microsporidia have been suggested to influence the composition of *Caenorhabditis elegans* genotypes and resistant strains can outcompete sensitive ones in just a

few generations [18–20]. In competition experiments with over a dozen isolates of *Daphnia magna*, different microsporidia species have been shown to select for specific strains [21,22]. Using genetic mapping, several genomic regions contributing to microsporidia resistance in *C. elegans*, *D. magna*, and honey bees have been identified [19,23–26].

C. elegans has become a powerful model for studying host-pathogen coevolution [27–30]. In the wild, *C. elegans* contend with bacterial, fungal, viral, and microsporidian pathogens and these coevolving species represent strong selective pressures on the animal's genome [31,32]. To facilitate the study of natural diversity, hundreds of isolates of *C. elegans* have been collected from around the world [33]. These wild isolates have different levels of susceptibility to pathogens and natural variants have been discovered that impact traits such as bacterial avoidance and viral susceptibility [7,19,34–37]. Although studying phenotypic variation in wild isolates is a powerful approach, measuring each strain individually is time consuming and laborious. To circumvent this issue, strategies have been developed to perform multiplex competitive fitness assays under selective conditions such as starvation stress or different bacterial diets [38–40]. Several sequencing-based approaches, termed either PhenoMIP or MIP-seq, determine the identity of these individual strains by using molecular inversion probes (MIPs) to enrich for their unique genomic signatures [39,40].

A common microbial infection found in wild *C. elegans* is from species of microsporidia in the *Nematocida* genus. Infection of *C. elegans* by microsporidia begins with ingestion of a chitin-coated spore [41]. The spore then fires its unique infectious apparatus, known as a polar tube, and deposits its sporoplasm within the host [42]. The sporoplasm then replicates to form membrane-bound, multinucleated cells know as meronts which then differentiate into spores that are shed by the host [16]. Some *Nematocida* species, such as *N. parisii*, *N. ausubeli*, and *N. ironsii*, infect only the intestine, while others, such as *N. displodere*, *N. ferruginous*, and *N. cider*, can proliferate in several tissues including the muscle and epidermis [15,19,41,43,44]. *C. elegans*

72 possesses several mechanisms to defend itself against microsporidia [45,46]. Infection with
73 microsporidia induces transcriptional upregulation of genes known as the Intracellular Pathogen
74 Response (IPR) [47]. Mutations in several negative regulators of the IPR cause elevated
75 expression of the IPR and resistance to microsporidia infection [48–50]. *C. elegans* also possess
76 a separate form of inherited immunity that is activated by infection of parents and is transferred
77 to progeny [49].

78 Here we present the results of a high-throughput fitness competition of 22 pooled *C. elegans* wild
79 isolates infected by four species of microsporidia at multiple doses. We identified 16 candidate
80 interactions of either host resistance or sensitivity. We demonstrate that the wild isolate JU1400
81 has distinct and opposing responses to infection by different microsporidia species. This strain
82 has a defect in tolerance to the epidermally-infecting *N. ferruginous* but is resistant to the
83 intestinal-infecting *N. ironsii* through specific elimination of infection by this species. Through
84 mapping experiments and the generation of recombinant strains, we demonstrate that the
85 opposing phenotypes of JU1400 are caused by separate loci. In contrast to the species-specific
86 phenotypes we observed from fitness competitions, transcriptional analysis showed a host
87 response to infection that is mostly independent of the microsporidia species, but dependent upon
88 the *C. elegans* strain. Notably, we identified a signature of down-regulated genes that has overlap
89 with the *C. elegans* response to toxins, and this downregulated response was most prominent in
90 the tolerance-defective strain JU1400 infected with *N. ferruginous*. Our results demonstrate that
91 PhenoMIP can efficiently identify resistant and sensitive wild isolates and that microsporidia
92 genotype-specific interactions are common in *C. elegans*.

93

94 **Results**

95 ***A PhenoMIP screen of wild isolate strains reveals diverse responses to microsporidia***
96 ***infection***

97 To identify *C. elegans* strains that vary in their resistance or susceptibility to microsporidia
98 infection, we carried out a modified PhenoMIP screen. We chose 22 *C. elegans* wild isolate strains
99 that are genetically diverse and isolated from a range of geographic regions (**Supplementary**
100 **Figure S1**). We selected four pathogenic microsporidia species that differ in their impact on *C.*
101 *elegans* development and the tissues they infect (*N. parisii*, *N. ausubeli*, and *N. ironsii* infect the
102 intestine and *N. ferruginous* infects the muscle and epidermis) (**Figure 1A and Supplementary**
103 **Table S1**) [15,16,19,43,51]. To synchronize infections, we treated adult populations with a sodium
104 hydroxide and sodium hypochlorite mixture (known as bleach synchronizing) and allowed the
105 recovered embryos to hatch in the absence of food. The process of bleach synchronizing animals
106 for microsporidia infection has been shown to have similar levels of infection between bleached
107 versus laid embryos, and short-term starvation is reported to have minimal impact on wild isolates
108 [19,20,40]. We pooled equal numbers of synchronized first larval stage (L1) wild isolates and a
109 laboratory reference-derived strain (VC20019) into a single population. VC20019, was chosen as
110 a reference because it has many genomic variants that can be used to distinguish it from N2 while
111 having developmental timing and fecundity similar to that of N2 [39,52]. We then plated these
112 animals along with their food source of *Escherichia coli* bacteria mixed with one of four doses of
113 each microsporidia species (high, medium, low, and none) (**Supplementary Table S2**). We
114 hypothesized that a high-dose exposure could identify *C. elegans* strains that were resistant or
115 tolerant to microsporidia infection while medium- and low-dose exposures might identify strains
116 exhibiting mild to strong susceptibility to microsporidia infection. Animals were exposed to
117 microsporidia spores for 72 hours at 21°C, before collecting and bleach synchronizing the
118 population. This mixture inhibits microsporidia from infecting the next generation of animals and
119 synchronizes the population [49]. This microsporidia-free population of L1s was then grown in the

absence of infection for 72 hours at 21°C to allow intergenerational immunity to reset [49]. Except for the *N. ausubeli* medium-dose infection replicates (**see Methods**), worms in each condition were infected for an additional three cycles for a total of eight generations. Adult animals were collected every two generations at the end of the uninfected phase and genomic DNA was isolated for further analysis (**Figure 1B**).

To determine how population composition changes due to exposure to microsporidia, we calculated the relative abundance of each strain within each condition. We used MIPs to target strain-specific variants for sequencing at high depth. In total we sequenced 127 samples, which is the equivalent of 2162 infections and 736 mock/control infections. From each of the eight mock-infection controls and twenty-four infection replicates for every strain we calculated a mean fold-change rate (FCR) from across all timepoints. The distribution of FCRs for each strain was then converted to a modified z-score distribution to identify candidate interactions (**See Methods**). From this dataset, we identified 16 nematode/microsporidia pairings where the modified z-score for both high-infection replicates was consistently outside the range of +/- 1.5 **(Figure 2, Supplementary Figure S2 and Table 1)**. We also generated mean growth profiles across all timepoints for each worm strain in environments that were either pathogen-free or infected by each of the microsporidia species (**Figure 3A and B**). From our analyses we observed ten interaction pairs with reduced population fitness (low-fitness strains), suggesting potential susceptibility to infection. In addition, we observed six interactions with increased population fitness (high-fitness strains), suggesting a potential resistance to infection conditions. Our high-fitness interaction set included the previously reported resistance interaction of CB4856 to *N. ironsii* (**Supplementary Figure S3**) [19,51] which further suggested our scoring threshold was appropriate for the detection of interactions in this assay format. Of the 15 novel candidate interactions, we identified five interactions with *N. ironsii* (ERTm5), eight with *N. ferruginous* (LUAm1), two with *N. ausubeli* (ERTm2), and no strong interactions with *N. parisii* (ERTm1). In

145 total, our screen yielded 13 *C. elegans* wild isolate strains with significant interactions, including
146 the strains JU360, JU1400, and MY2 that had interactions with more than one species of
147 microsporidia (**Figure 2 and Table 1**).

148 **JU1400 fails to tolerate *N. ferruginous* infection**

149 To validate a subset of our large-scale multiplex identification of microsporidia-strain phenotypes,
150 we performed isogenic population infection experiments. We infected individual strains with doses
151 of microsporidia spores equivalent to those used in the PhenoMIP experiment (**Figure 3C and D**
152 **and Supplementary Figures S4-S6**). We examined a combination of phenotypes including
153 morphology of adult populations, formation of microsporidia meronts or spores, and embryo
154 production. Most high-fitness strains tended to experience a smaller reduction in embryo
155 production ratios compared to changes in lab reference N2 in identical infection conditions. Low-
156 fitness strains, on the other hand, experienced developmental delay phenotypes and/or a
157 reduction in fecundity–both of which would contribute negatively to the fitness readout observed
158 via PhenoMIP. These phenotypes were most evident in JU1400 and MY1 which both had severe,
159 dose-dependent responses to infection by the epidermal microsporidia species *N. ferruginous*
160 (**Figure 3C and D and Supplementary Figure S7**). In total, of the 12 pairs that we observed
161 (**Table 1**), nine had altered relative fecundity profiles that could account for the fitness changes
162 observed from our PhenoMIP screen. Additionally, of the seven pairs we retested that had a z-
163 score below -1.5, six had a significant reduction in embryos when infected, compared to N2.

164 To examine how a *C. elegans* strain responds to different microsporidia species, we focused on
165 JU1400, in which we observed reduced fitness to infection by both *N. ferruginous* and *N. ironsii*.
166 To determine why JU1400 appeared sensitive to *N. ferruginous*, we performed pulse-chase
167 experiments by infecting animals for 3 hours, washing away free spores, and replating animals
168 for an additional 69 hours [19]. We observed that the percentage of JU1400 and N2 animals
169 infected with *N. ferruginous* was similar (**Figure 3E and Supplementary Figure S8A and B**).

170 Additionally, the amount of meronts formed during infection did not significantly differ between N2
171 and JU1400 (**Figure 3F and Supplementary Figure S8C and 8D**). Taken together, these results
172 demonstrate that although JU1400 is more sensitive to the effects of *N. ferruginous*, JU1400 is
173 not significantly more infected, suggesting a defect in tolerance.

174 To determine the specificity of JU1400 to *N. ferruginous* infection, we infected JU1400 with other
175 related microsporidia species and strains. We infected JU1400 with a second isolate of *N.*
176 *ferruginous,* LUAm3, as well as a separate muscle and epidermal-infecting microsporidian, *N.*
177 *cider* [44]. Infection by LUAm3 caused the same severe phenotype as LUAm1 (**Supplementary**
178 **Figure S9A and B**). JU1400 is infected by *N. cider* to a similar extent as N2, but infection by this
179 species resulted in a dose-dependent reduction in embryo numbers in JU1400 that was not
180 observed in N2 (**Supplementary Figure S9C and D**).

181 **JU1400 specifically clears *N. ironsii* infection**

182 In addition to the verified susceptibility to *N. ferruginous,* our PhenoMIP screen also identified a
183 more moderate fitness disadvantage for JU1400 in high-dose exposures to *N. ironsii* (**Figure 3A**).
184 We infected N2 and JU1400 with *N. ironsii* for 72 hours and compared the relative change in
185 embryos for each strain versus mock-infected controls. We observed no significant difference in
186 this normalized number of embryos between the N2 and JU1400 strains (**Figure 4A**). However,
187 JU1400 is significantly less infected, suggesting that JU1400 is resistant to *N. ironsii* infection
188 **(Figure 4C and Supplementary Figure S10A and C)**. To determine whether the observed
189 resistance conferred a fitness advantage at a later time point, we exposed JU1400 animals to *N.*
190 *ironsii* for 96 hours and observed significantly more embryos and significantly less infection
191 compared to N2 (**Figure 4B and D and Supplementary Figure S10B and D**). Together our data
192 suggest that although JU1400 appears to have a short-term disadvantage in our pooled
193 competition assays, this strain has a long-term advantage due to enhanced resistance towards
194 *N. ironsii*.

195 Several mechanisms of *C. elegans* resistance to microsporidia infection have been described,
196 including a block of invasion or clearance of infected parasite [19,20,49,51]. To determine how
197 JU1400 is resistant to *N. ironsii* infection, we performed a pulse-chase experiment by infecting
198 animals for 3 hours, washing away any external microsporidia spores, and examining animals at
199 3, 24, and 72 hours post infection (hpi). Both N2 and JU1400 had similar numbers of sporoplasms
200 at 3 hpi, but JU1400 had decreased levels of pathogen at both 24 and 72 hpi (**Figure 5A**). This
201 experiment revealed that JU1400 does not block microsporidia invasion, but instead has the
202 capability to actively eliminate *N. ironsii* infection. To determine if the resistance in JU1400 was
203 dependent upon development stage, we performed pulse-chase infections at the L4 stage and
204 observed that JU1400 animals could no longer clear the infection (**Figure 5B**).

205 Resistance to *N. ironsii* has previously been observed in the *C. elegans* wild isolate, CB4856 [19].
206 This resistance was shown to occur through a modest decrease in invasion coupled with the
207 ability to clear the infection at the L1 stage. To compare the properties of these two resistant
208 strains, we infected both strains with *N. ironsii* for 72 hours. This experiment shows that JU1400
209 is more resistant to infection **(Figure 5C**). To determine the specificity of JU1400 resistance, we
210 tested infection with either *N. parisii* or *N. ausubeli* for 72 hours. CB4856 was slightly, but not
211 significantly less infected by *N. parisii* and *N. ausubeli,* whereas JU1400 was infected by these
212 species to the same extent as N2 (**Figure 5D**). We also tested the ability of JU1400 and CB4856
213 to clear microsporidia infection, and both strains could only eliminate *N. ironsii* (**Supplementary**
214 **Figure S10E and F**). Together, these results demonstrate that JU1400 resistance is specific to
215 *N. ironsii*.

216 The immunity of JU1400 against *N. ironsii* could be a specific recognition of *N. ironsii* infection
217 that induces broad immunity towards microsporidia or the immunity itself could be specific for *N.*
218 *ironsii*. To distinguish between these possibilities, we set up coinfection experiments using
219 species-specific FISH probes and then coinfected JU1400 and N2 animals with *N. ausubeli* and

220 either *N. ironsii* or *N. parisii*. Under these conditions, *N. ironsii* sporoplasms are eliminated
221 regardless of the presence of *N. ausubeli*. There is no clearance of *N. ausubeli* observed, either
222 by itself or in the presence of *N. ironsii*. (**Figure 5E and Supplementary figure S11A and B**). No
223 clearance was observed in N2 regardless of the infection condition (**Supplementary Figure**
224 **S11C**). These results further demonstrate that JU1400 has specific immunity towards *N. ironsii*.

225 ***Genetic mapping reveals multiple loci are responsible for the interactions of JU1400 with***
226 ***microsporidia***

227 The opposing phenotypes of JU1400 in response to microsporidia infection could be caused by
228 the same or different genetic loci. To determine the genetic basis for JU1400 being sensitive to
229 *N. ferruginous* and resistant to *N. ironsii*, we mapped the causative alleles using a pooled
230 competitive fitness assay [52]. We crossed JU1400 to the mapping strain VC20019 and infected
231 F2 animals with either *N. ferruginous* for 72 hpi or *N. ironsii* for 96 hpi **(Supplementary Table S3**
232 **and Methods**). After two rounds of selection, genomic DNA was isolated from each sample and
233 MIP-MAP sequencing libraries were generated [52]. As a control, we used this approach to map
234 the resistance of CB4856 to *N. ironsii.* We then compared our results to a previous study that
235 determined regions responsible for resistance [19]. Although the previous mapping study was
236 based on pathogen load as opposed to our mapping of competitive fitness advantage, several
237 regions mapped concordantly between the two approaches on chromosome II and the right arm
238 of chromosome V (**Supplementary Figure S12)**.

239 Our mapping results of JU1400 with *N. ferruginous* identified a single peak of VC20019 marker
240 fixation on the left-hand side of chromosome I (**Figure 6A**). This mapping was repeated with MY1,
241 another strain that exhibited a fitness disadvantage with *N. ferruginous* **(Figure 3B-D)**. The
242 mapped region under negative selection was the same in MY1. The MY1 strain also carries the
243 *zeel-1/peel-1* incompatibility locus at chromosome I, which accounts for the specific signal seen
244 at the I:2,726,021 marker in both the infected and uninfected samples (**Supplementary Figure**

245 **S13A)** [53]. To determine if the same locus was responsible for *N. ferruginous* in MY1 and
246 JU1400, we tested their ability to complement. First, we determined that both MY1 and JU1400
247 display a recessive phenotype when crossed to our control strain. We then mated MY1 and
248 JU1400 and the resulting cross progeny were susceptible to *N. ferruginous* infection, indicating
249 that the two strains do not complement (**Supplementary Figure S14A and B**). We then infected
250 MY1 with *N. ironsii*. There were fewer MY1 animals containing spores compared to N2, and less
251 JU1400 animals had spores or meronts compared to MY1 animals (**Supplementary Figure S14C**
252 **and D**). Together this data suggests a region on the left side of chromosome I, is responsible for
253 sensitivity to *N. ferruginous* in multiple strain*s*.

254 Our mapping of JU1400 with *N. ironsii* at 96 hours identified three regions that are linked with
255 resistance to infection, one on the left-hand side of chromosome II from 1,639,865-4,426,687, a
256 second in a broad area of chromosome V from 11,035,658-18,400,066, and a third on the right-
257 hand side of chromosome X from 15,180,772-17,676,467 (**Figure 6B**). A similar pattern was
258 observed when these mapping experiments were performed at 72 hours, with the exception that
259 the region on chromosome X was no longer observed (**Supplementary Figure S13B**). We also
260 observed a region on the left side of chromosome I where JU1400 variants underwent weak
261 negative selection upon over multiple *N. ironsii* infection rounds. Together, our data suggests that
262 JU1400 resistance to *N. ironsii* is multigenic and may be influenced by infection time.

263 To confirm that the region on chromosome I was responsible for sensitivity to *N. ferruginous*
264 infection, we generated Near Isogenic Lines (NILs). These NILs were constructed by crossing a
265 version of VC20019 that contained a CRISPR-integrated single-copy GFP on chromosome I
266 (AWR133) (**Supplementary Figure S15A**). We tested ten independent NILs that contained at
267 least some JU1400 sequence to the left of I:2,851,000. All ten of these NILs were sensitive to
268 infection by *N. ferruginous* (**Supplementary Figure S15B).** We used molecular markers to
269 genotype these NILs, mapping the susceptibility locus to I:1-1,051,810 (**Supplementary Table**

270 **S4**). We then outcrossed one of these NILs, AWR140 back to N2 six times. During this outcrossing
271 process, we recovered two lines, AWR144 and AWR145, that contained different responses to
272 *N. ferruginous* infection (**Figure 6D**). We performed whole-genome sequencing of AWR138
273 (another independently isolated NIL), AWR140, AWR144, and AWR145 which narrowed the
274 critical region of association for our phenotype to I:1-701,078 (**Figure 6C**). Within this region, we
275 identified 12 genes shared between JU1400 and MY1 (same complementation group) but absent
276 in ED3042 and JU360 which tested into separate complementation groups **(Supplementary**
277 **Table S5**). The NIL AWR145 is sensitive to *N. ferruginous* infection but is only partially resistant
278 to infection by *N. ironsii* (**Figure 6D and E).** Together, our data demonstrate that the *N.*
279 *ferruginous* sensitivity and *N. ironsii* resistance to JU1400 are determined by distinct genetic loci.

280 ***Transcriptional analysis of the JU1400 response to microsporidia infection***

281 To determine how the JU1400 strain differs in its response to microsporidia infection, we
282 performed transcriptional analysis. We grew three biological replicates of N2 and JU1400 L1
283 stage animals either without microsporidia or infected with one of *N. parisii*, *N. ironsii*, *N.*
284 *ferruginous*, or *N. ausubeli* for 48 hours. We then extracted and sequenced the *C. elegans* and
285 microsporidia mRNA. First, we mapped the microsporidia mRNA in each of the eight infected
286 samples. For the three intestinal infecting species, between ~1-9% of reads were mapped for
287 each sample, with the exception of *N. ironsii* in JU1400, where few reads were identified, which
288 is consistent with this strain being resistant to this species. For *N. ferruginous*, fewer reads were
289 observed in either strain compared to the intestinal species, which is consistent to what we
290 observed by microscopy (**Supplementary Figure S16 and Supplementary Table S6**).

291 We then sought to determine how the two *C. elegans* strains responded to the four different
292 microsporidia species (**Supplementary Table S7)**. First, we used principal component analysis
293 (PCA), and projected samples back onto the two principal components which accounted for more
294 than 80% of the variance in our samples. PCA analysis revealed a clear clustering between the

295 two strains (**Figure 7A)** and a secondary analysis by strain clustered the uninfected samples
296 against pathogen infected samples (**Supplementary Figure S17**). Second, we clustered the
297 differential expression profiles of the eight infected samples. This approach revealed several large
298 groups of genes that were differentially expressed either across most samples or within the same
299 strain **(Figure 7B** and **Supplementary Table S8).** Although the largest difference in the samples
300 is between the two strains, we observe significant correlation between strains infected with each
301 microsporidia species (**Supplementary Figure S18**).

302 We then determined the properties of genes that are differentially regulated in each sample**.** The
303 number of differentially upregulated or downregulated genes ranged from 6-819, with the most
304 being in JU1400 infected with *N. ferruginous* **(Figure 7C).** We then classified differentially
305 expressed genes into either conserved, microsporidia species (pathogen) specific, *C. elegans*
306 strain specific, or strain-pathogen specific categories **(Figure 7D)**. We identified 97 genes
307 upregulated in all samples, and no genes that were broadly downregulated. We identified ~30-50
308 differentially expressed genes specific to either *N. ausubeli* or *N. ferruginous* infection, one gene
309 specific to *N. parisii* infection, and no genes specific to *N. ironsii* infection. We also observed 45
310 or more differentially upregulated genes that were specific to either N2 or JU1400. To determine
311 the types of differentially expressed genes in these samples, we annotated them using a set of
312 domains previously observed to be regulated during microsporidia infection [47,48,54]
313 (**Supplementary Table S9)**. About 35% of the conserved response were genes containing these
314 domains, with the most frequent being PALS, F-box, and MATH/BATH domains. About 25% of
315 the strain-specific genes also contained these domains, with each strain having at least one
316 PALS, F-box, and MATH/BATH, c-type lectin, and skr domain-containing gene expressed that is
317 specific to that strain **(Figure 7D and Supplementary Table S10)**. Skp-related proteins (*skr*) in
318 *C. elegans* were shown to bind to CUL-6 to ubiquitylate specific proteins [55]. *skr-4* is upregulated
319 in both host strains infected by all microsporidia species. Among the upregulated genes, we also

320 observe strain-specific *skr* genes such as JU1400 specific *skr-6*, and N2 specific *skr-5*
321 (**Supplementary Table S8)**.

322 To understand how transcriptional responses correlated with resistant and susceptible
323 phenotypes, we analyzed genes that were specifically regulated in JU1400 when infected with
324 either *N. ironsii* or *N. ferruginous* **(Figure 7D)**. Surprisingly, we only observed three differentially
325 expressed genes specific to *N. ironsii* infection of JU1400. In contrast, we saw 181 upregulated
326 and 266 down-regulated genes specific to *N. ferruginous* infection of JU1400. Many of the
327 upregulated genes contained domains enriched in the IPR. The down-regulated genes contained
328 a few genes with IPR domains, as well as 23 genes with cuticle collagen domains. These proteins
329 with collagen domains were especially striking, as we never identified more than one of these
330 genes having altered expression in any of the other gene sets.

331 To determine if other stresses had similarities to the response of JU1400 to *N. ferruginous*, we
332 compared the set of genes specifically differentially expressed in this sample to previously
333 published *C. elegans* transcriptional datasets [56]. We identified the top ten chemical or microbial
334 treatment data sets that had the most significant overlap with JU1400 infected by *N. ferruginous*
335 (**Supplementary Table S11)**. We then determined the overlap of these data sets to all our
336 samples (**Figure 7E-F and Supplementary Table S12).** This revealed that genes differentially
337 downregulated in JU1400 in response to *N. ferruginous* infection overlapped significantly with
338 treatments of chemical poisons such as pesticides (fenamiphos and dichlorvos), organic
339 compounds (acrylamide and tert-butyl hydrogen peroxide), and heavy metals (mercury and
340 cadmium). All of these treatments were previously shown to inhibit development or the production
341 of progeny in *C. elegans* [57–60]. We also observed significant overlap of the response to these
342 chemicals with JU1400 infected with *N. ironsii*, and both strains infected with *N. ausubeli*. These
343 three infected samples along with JU1400 infected with *N. ferruginous* also contained the largest
344 number of significantly down-regulated genes **(Figure 7C and Supplementary Figure S19).**

345 Additionally, we observed significant overlap of these four microsporidia infected samples to
346 pathogenic bacteria or toxins including *Staphylococcus aureus*, *Serratia marcescens*, *Bacillus*
347 *thuringiensis*, *Xenorhabdus nematophila*, and *Pseudomonas aeruginosa* (**Figure 7E-F**). These
348 patterns of transcriptional overlap were the most striking with differentially downregulated genes,
349 although some overlap with upregulated genes was also observed (**Supplementary Figure S20**).

350 We also performed enrichment analysis of our transcriptional data sets, observing that the
351 upregulated genes are commonly enriched for metabolic processes and signalling pathways**.** In
352 contrast, down regulated genes are enriched for proteolysis, fatty-acid related metabolic
353 processes and drug metabolism (**Supplementary Tables S13 and S14).** We also analyzed the
354 12 candidate genes within the mapped chromosome I region that contain genetic variants in both
355 JU1400 and MY1. None of these genes are differentially regulated in JU1400 upon *N. ferruginous*
356 infection.

357 **Discussion**

358 Animal populations often have genetic diversity to bacterial, viral, and fungal pathogens, but less
359 is known about how microsporidia infection influences host variation [5,6]. To investigate how
360 different microsporidia species impact genetic diversity, we measured the phenotypic responses
361 to infection in a collection of genetically diverse *C. elegans* wild isolates. A total of 13 out of 22
362 wild isolate strains displayed a significant difference in population fitness after microsporidia
363 infection when compared to the population as a whole. We detected these interactions among
364 three of the four microsporidia species we measured, with *N. ironsii* and *N. ferruginous* accounting
365 for the bulk of the fitness interactions observed. We attributed these fitness changes as signatures
366 of susceptibility (fitness decreases) or resistance (fitness increases) with respect to microsporidia
367 infection.

368 So far, the causative gene for any host variants that influence microsporidia interactions has not
369 been identified. Previous genetic mapping in *C. elegans*, *D. magna*, and honey bees have
370 revealed 3-6 loci involved in resistance and sensitivity to microsporidia [19,23–26]. Additionally,
371 some loci in *D. magna* appear to be specific to different microsporidia species, which we show to
372 be the case for JU1400 [24]. Our genetic analysis of JU1400 identified that susceptibility to *N.*
373 *ferruginous* in both JU1400 and MY1 mapped to a single region on the left arm of chromosome I
374 while the resistance phenotype of JU1400 to *N. ironsii* appears to be caused by at least three
375 genomic regions. Taken together, our results add to the increasing evidence that suggests that
376 microsporidia have had a major impact on the evolution of animal genomes.

377 Microsporidia infect a wide diversity of animal phyla and infections are highly prevalent [12,13,61].
378 Nine species of microsporidia have been reported to infect *C. elegans*, with four having been
379 found in wild isolates and five capable of infecting *C. elegans* after isolation of microsporidia from
380 other nematode species [15,19,32,41]. The most common are the intestinal-infecting *N. parisii*
381 and *N. ausubeli,* which have been found in Europe, the United States, India, and Africa. The
382 geographical relationships between the strongest interactions we detected is not clear; JU1400
383 was isolated in Spain, *N. ironsii* in Hawaii, and *N. ferruginous* in France. Although host genetic
384 factors were shown to be responsible for the geographic range of a microsporidian infecting *D.*
385 *magna*, further work is needed to understand if there is a geographic basis to microsporidia
386 resistance and susceptibility in *C. elegans* [62].

387 Pathogen tolerance is being increasingly appreciated as a valuable way for hosts to improve
388 fitness in the presence of pathogens, although these mechanisms are less understood [63].
389 Tolerance is generally defined as the ability of a host to limit the consequences of a given level of
390 infection [64]. Here we show that JU1400 is very sensitive to infection by two different epidermal
391 infecting microsporidian species, but this strain does not display significantly higher levels of *N.*
392 *ferruginous* infection than non-sensitive control strains. RNA-seq analysis reveals that JU1400

393 has a unique response to microsporidia when infected with *N. ferruginous*. This response shares
394 similarities to several chemical toxins and pathogens that have been shown to damage *C.*
395 *elegans*. Although the mechanistic basis of this transcriptional similarity is likely different between
396 the various conditions, this result suggests that JU1400 infected with *N. ferruginous* has a
397 response similar to worms being exposed to toxic conditions. This signature is also detected to a
398 lesser extent in other strain-microsporidia pairings that cause developmental delay, including *N.*
399 *ausubeli* with either strain or *N. ironsii* with JU1400 [16]. Thus, one potential consequence of the
400 lack of tolerance to *N. ferruginous* is a developmental delay. Consistent with this result is the
401 observation of many genes containing collagen domains being down regulated in JU1400 infected
402 with *N. ferruginous*. Further work uncovering the genetic variant responsible for this aberrant
403 response will help elucidate the mechanistic basis of tolerance to microsporidia infection. None
404 of the differentially regulated genes are among the list of 12 candidate genes in the critical region
405 of chromosome I for *N. ferruginous* sensitivity, suggesting that causative gene or variant is not
406 differentially regulated during infection.

407

408 Our initial observation from our PhenoMIP experiment is that JU1400 has severely reduced
409 fitness when infected with *N. ferruginous* and a moderate reduction of fitness when infected with
410 *N. ironsii* (**Figure 3A**). In our follow up experiments using embryo counts as a proxy for fitness,
411 we observed that at 72 hours there was no relative difference in reduction of embryos during
412 infection with *N. ironsii* (**Figure 4A**) and significantly less reduction of embryos in JU1400 at 96
413 hours (**Figure 4B**). However, we also observed a decrease in embryos at 72 hours when JU1400
414 was infected with *N. ironsii* compared to N2 or VC20019 (**Supplementary Figure S4B**). We also
415 performed MIP-MAP experiments using similar conditions to those in our initial PhenoMIP
416 experiment. These experiments showed that JU1400 regions were selected for at both 72 hours
417 (**Supplementary Figure S13B**) and at 96 hours (**Figure 6B**). Regions on both chromosome II

418 and chromosome V were selected for at both times, but only the region on the X chromosome
419 was selected for at 96 hours. In addition to our experiments on host fitness, we also provide strong
420 evidence that there is resistance to *N. ironsii* in JU1400 due to its ability to clear the parasite.
421 Thus, our evidence is supportive of a model where JU1400 is resistant to *N. ironsii* infection and
422 has increased fitness compared to control strains at a 96-hour time point. Our data is inconclusive
423 about the impact of *N. ironsii* on JU1400 at 72 hours as we have conflicting results depending on
424 the experiment. Our results suggest that a limitation of our PhenoMIP experiment is that
425 resistance to microsporidia infection doesn't always result in a fitness advantage under certain
426 conditions. Our data also suggests that future competitive selection experiments using
427 microsporidia could be improved using 96-hour selections to identify resistant strains.

428 JU1400 is resistant to *N. ironsii* infection by clearing the invaded parasite. This immune
429 mechanism is similar to previous results seen in *N. ironsii* infection of CB4856. However, the
430 immunity in JU1400 results in less infection than in CB4856. The JU1400 resistance mechanism
431 is specific, as the clearance we observe does not occur in even the closely related sister species
432 *N. parisii*, which shares 92% identical DNA [43]. A strain of mosquito that is resistant to infection
433 by a parasitic nematode was shown to rely on activation of an upregulated immune response [65].
434 However, we see no evidence for an increased transcriptional response of JU1400 in response
435 to *N. ironsii*. A potential caveat to these experiments is that we infected JU1400 at the L1 stage,
436 but measured the transcriptional response at the L4 stage, a stage where if infections are initiated,
437 parasite clearance is not observed. We do, however, observe additional parasite clearance
438 between 24 and 72 hours (**Figure 5A**), which corresponds to between the L2/L3 stages and
439 adults, suggesting that if there was transcriptional signature of resistance, it would be observed
440 under our experimental RNA-seq conditions. Instead of a specific transcriptional response of
441 JU1400 to *N. ironsii*, we observe a *C. elegans* strain-specific response of immune genes including
442 upregulation of several CHIL genes, which have been observed to be upregulated in response to

443 epidermally infecting oomycetes, but have not previously been observed in response to
444 microsporidia infection [66,67]. This strain-specific-response of *C. elegans* has also been
445 observed with several bacterial pathogens, suggesting that there exists a diversity of innate
446 immune responses within the *C. elegans* population [68]. We also observe more strain-specific
447 regulated genes than pathogen-specific regulated genes, suggesting that *C. elegans* responds
448 similarly to infection by different species of *Nematocida* [69].

449 Here we demonstrate that PhenoMIP can be used to identify variants of pathogen infection in a
450 high-throughput manner. We compressed the equivalent of 2898 individual infection experiments
451 into 127 pooled population experiments, allowing a large savings in time and reagents required
452 for this study. The genomic loci responsible for these phenotypes can then be identified using
453 MIP-MAP [52]. We only tested a small fraction of the current *C. elegans* isotypes identified,
454 suggesting there is much variation to microsporidia within *C. elegans*. Our pooled selection
455 approach could also be applied to other *C. elegans*-related microbes such as those isolated from
456 the *C. elegans* microbiome or known pathogens and viruses [70,71]. Here we studied the animal's
457 reproductive fitness, but our approach could be modified, for instance, to select for pathogen load
458 using fluorescently labelled pathogens. The wild isolate collections of *C. elegans* provide a unique
459 opportunity to study how animals evolve in response to infection. The *Caenorhabditis elegans*
460 Natural Diversity Resource (CeNDR) collection, hosts more than 1500 wild isolate strains across
461 550 isotypes [33]. Based on our initial results, many of these strains are likely to have fitness
462 interactions with microsporidia infection. Identifying additional sensitive or resistant strains would
463 drive the discovery and further elucidation of evolved mechanisms of host-responses in
464 coevolving pathogens.

465 **Acknowledgements**

466 We thank Hala Tamim El Jarkass and Keir Balla for providing helpful comments on the
467 manuscript. We thank John Calarco for the kind gift of plasmids to perform CRISPR and Robert

468 Waterston and Donald Moerman for the kind gift of reagents to perform PhenoMIP and MIP-MAP.
469 This work was supported by Canadian Institutes of Health Research grants no. 400784 and
470 461807 and an Alfred P. Sloan Research Fellowship FG2019-12040 to A.W.R. and by NIH grant
471 R35 GM146836 to R.J.L. Some strains were provided by the CGC, which is funded by NIH Office
472 of Research Infrastructure Programs (P40 OD010440) and we thank WormBase.

473 **Author contributions**

474 C. M. and A. W. R. conceived of the project. C. M., M. A. X., Y. C. W., and A.R.W. designed and
475 analyzed the experiments and cowrote the paper, with consolation from all the authors. C. M., M.
476 A. X., W.Z., and S. M.A. conducted experiments. R. J. L. provided novel reagents. A.W.R.
477 provided funding and mentorship.

478 **Competing Interests**

479 The authors declare that they have no competing interests.

480

481 **Methods**

482 ***Nematode maintenance and worm pooling***

483 Nematode strains were maintained at 21°C on a modified version of nematode growth media
484 NGM) with a 1:1 ratio of Agar:Agarose to reduce burrowing by wild isolate strains. NGM plates
485 were seeded with OP50-1 bacteria grown to saturation overnight in lysogeny broth (LB) at 37°C
486 and concentrated to 10X. All wild isolate strains used (**Supplementary Data S1**) are available
487 from the CGC. The AWR133 mapping strain was generated from VC20019 by inserting a GFP at
488 I:2,851,135 using CRISPR-based homologous recombination [72]. Nematode strains were grown
489 continuously without any starvation or contamination for a minimum of two weeks before seeding
490 individual strains to two 15-cm NGM plates seeded with 1.5 ml of 40X concentrated OP50-1. After

491 96 hours, gravid adult populations were bleach-synchronized [73] and allowed to hatch into axenic
492 M9 media for ~16 hours at 20°C. Synchronized L1 samples were counted and equal numbers of
493 animals were mixed into a single population before redistributing ~13,000 L1s to each 15-cm
494 NGM experimental plate with a mixture of 1.5 ml of 40X OP50-1 and the appropriate amount of
495 spores as needed (**Supplementary Table S2**).

496 ***PhenoMIP competitive assays***

497 PhenoMIP competitive assays were based on a previously described protocol [39]. We modified
498 this method to use bleach-synchronization between generations to directly measure egg-
499 production as an output of population fitness. At each generation, samples were bleach-
500 synchronized as gravid adults ~72 hours after plating L1s and incubating at 21°C. Bleached
501 embryos were then allowed to hatch over 18-22 hours while incubating on a shaker at 21°C in
502 axenic M9 media. Each sample was gently pelleted and 3 – 7 µl of each pellet was used to seed
503 the experimental plate for the next generation of animals. Overall, the competitive assay consisted
504 of four total cycles, with one infection generation and one uninfected (resting) generation per
505 cycle. For each infection cycle, 3 ml of 40X OP50-1 culture was mixed in 15-ml falcon tubes with
506 twice the indicated dose of spores used on each infection experiment before splitting the mixture
507 to each duplicate plate. Worm populations for each specific replicate were then added to the plate
508 and samples were distributed evenly across the NGM surface before drying. For each rest cycle,
509 worm pellets were plated onto 15-cm NGM plates previously seeded with 1.5 ml of 40X OP50-1
510 culture. Prior to bleach-synchronizing the 72h-resting generation, a subsample of the population
511 was collected and frozen as a genomic DNA source. Microsporidia doses were adjusted after the
512 first infection round in order to ensure high enough selection pressure throughout the population
513 without causing the populations to become completely infertile or developmentally arrested
514 (**Supplementary Table 2**) [74]. The initial infection round with *N. ausubeli* caused animals on the
515 high-dose plates to produce no progeny. Therefore, the medium-dose infection series became

516 the high-dose series at 53,000 spores/cm^2. A new medium-dose series was started using an
517 uninfected control replicate population from the first rest phase. This new medium-dose series
518 (39,800 spores/cm^2) therefore only experienced three rounds of infection selection of *N. ausubeli*.

519 ***PhenoMIP sequencing and analysis***

520 PhenoMIP sequencing libraries were generated using previously designed MIPs for the wild
521 isolate strains from the Million Mutation Project [39]. Individual MIPs were normalized to a
522 concentration of 100 µM and pooled to a maximum volume of 85 µl. 10 µl of 10X Polynucleotide
523 Kinase (PNK) Buffer and 5 µl of PNK were added to a volume of 85 µl pooled MIPs before
524 incubating for 45 minutes at 37°C and 20 minutes at 80°C. This pool was then diluted to a working
525 concentration of 330 nM. Libraries were generated using 160 ng of genomic DNA from each
526 sample and generated as previously described [52]. Libraries were sequenced on an Illumina
527 NextSeq system with each PhenoMIP library ranging between 0.0882×10^6 and 2.723×10^6 reads
528 and a mean of 9566 ± 7994 reads per probe.

529 For each sequencing library, reads were initially analysed as previously described [52] with the
530 exclusion of the normalization step for each MIP. After the abundance of each MIP was calculated,
531 an average abundance was calculated for each strain as well as a standard deviation across this
532 average. These values were used in downstream analysis of population structure across multiple
533 timepoints.

534

535 Population structure and fold-change analysis was calculated across each experiment using the
536 amalgamated data from above. Strains with a starting abundance value below 5×10^{-3} (CB4854
537 and JU312) were eliminated from downstream population analysis. Remaining data were further
538 transformed with any values below 1.0×10^{-3} being converted to this value to accommodate $\log_2$
539 growth analysis. Total fold-change and mean fold-change were calculated based on starting and
540 end-point changes in abundance versus total generations (two generations per infection cycle).

541 In samples with negative trajectories, however, the final generation of growth was calculated as
542 the first instance of abundance at or below the lower limit of 1.0×10^{-3}. Mean fold-change rate was
543 calculated based on the total fold-change abundance in the final generation of growth divided by
544 the expected number of generations passed. Each experimental condition may have had multiple
545 biological replicates (referred to in text as replicates), each with a time series of samples. Each
546 fold-change rate calculated for a single time series represented a single replicate. Mean fold-
547 change rate for each strain was therefore a combination of multiple replicates across multiple
548 experimental conditions (**Supplementary Data S1**).
549
550 Given the nature of the smaller datasets and the expectation of potential outliers stretching out
551 the tails of the mean FCR distribution, modified z-scores were calculated using the following
552 formula where $\tilde{Y}$ is the median of the data and $MAD = median(|Y_i - \tilde{Y}|)$
553
554 $$M_i = \frac{0.6745(x_i - \tilde{x})}{MAD}$$
555
556 To identify outliers and potential interaction candidates, we used a minimum z-score of ± 1.5 as
557 our threshold where both replicate samples were each required to meet the threshold.

558 ***Microsporidia infection assays***

559 Continuous microsporidia infection assays were conducted using ~1,000 bleach-synchronized
560 L1s obtained from cultures rotating at 21°C for 18-22 hours. Worm populations were pre-mixed
561 in a 1.5 ml microfuge tube with 400 µl of 10X OP50-1 and microsporidia spores (**Supplementary**
562 **Table S2**). Samples were then spread onto individual unseeded 6-cm NGM plates and allowed
563 to dry before incubating at 21°C. Plate populations were imaged using a
564 Leica S9i Stereomicroscope before fixing samples for microscopy. Animals were washed in

565 M9/0.1% Tween-20 at least three times before fixing with acetone. Chitin staining for
566 microsporidia and embryos was performed using Direct Yellow 96 [75]. Meronts and sporoplasms
567 were visualized using FISH probes conjugated to CAL Fluor Red 610 (LGC Biosearch
568 Technologies). *N. ferruginous* was stained using 3 ng/ul of a mix of three CAL Fluor Red 610
569 probes designed to target the 18S rRNA: GTTGCCCGCCCTCTGCC,
570 CTCTGTCCGTCCTCGGCAA, and CGGTCTCTAATCGTCTTC. For pathogen-specific staining,
571 MicroF-CAL Fluor Red 610 (AGACAAATCAGTCCACGAATT) was used for *N. parisii* and
572 Microsp1A-FAM (CAGGTCACCCCACGTGCT) was used for *N. ausubeli*. Unless otherwise
573 noted, all remaining FISH probes used 5 ng/µl of MicroB, a *Nematocida* microsporidia 18S rRNA
574 sequence: CTCTCGGCACTCCTTCCTG [15]. Stained samples were mixed with Biotium
575 EverBrite mounting medium with DAPI before mounting on slides for quantitation.

576 ***Embryo analysis and normalization***

577 Unless otherwise noted, embryo analyses were completed using normalized values which were
578 calculated in the following manner. For each replicate experiment, the uninfected control for each
579 strain was used to establish a baseline mean embryo value $(\bar{Y})$. Embryo counts for individual
580 animals (Y) of the same strain within the same replicate experiment were normalized $(Y/\bar{Y})$ before
581 combining with the normalized values from matching replicate experiments. This normalization
582 step facilitated the analysis of relative changes to embryo production, rather than absolute
583 changes in embryo counts which could vary both between nematode strains and replicate
584 experiments. The combined normalized populations were compared using two-way ANOVA with
585 a Tukey HSD post hoc.

586 ***Microscopy and image quantification***

587 All imaging was done using an Axio Imager.M2 (Zeiss) and captured via ZEN software under
588 identical exposure times per experiment. Animals containing clumps of spores visible in the body

589 after 72 hours by DY96 straining were considered as 'new spore formation'. Animals with one
590 sporoplasm or more in intestinal cells stained with FISH were considered infected. Gravidity of
591 worms was determined by counting the number of embryos per hermaphrodite animal.

592 Pathogen burden and body size was determined using ImageJ/FIJI software [76]. Individual
593 worms were outlined as "region of interest" with selection tools. Body size of worms were
594 determined using the "measure area" function. To quantify fluorescence (pathogen burden),
595 signal from FISH staining was subjected to the "threshold" function followed by "measure percent
596 area" tool.

597 ***Pulse-chase assays***

598 Pulse-chase assays were performed on 6-cm NGM plates with roughly 6,000 bleach-
599 synchronized L1s obtained from cultures rotating at 21°C for 18-22 hours. Worm populations were
600 first premixed in a 1.5 mL microcentrifuge tube with 5 µL of 10X OP50-1 and 1.25 million spores
601 per microsporidia strain. This dose was chosen to produce N2 controls with 85-90% infection
602 rates at 3 hpi. Samples were then spread onto individual 6-cm NGM plates and allowed to dry
603 before incubating at 21°C for 3 hours. To subsample the population at 3 hpi, plates were washed
604 at least two times with M9 in a 1.5 mL microcentrifuge tube to remove OP50-1 and residual
605 spores. Half the population was then fixed in acetone and stored at -20°C. The other half was
606 mixed with 50 µL of 10X OP50-1 and plated onto 6-cm NGM plates. Samples were then incubated
607 at 21°C for 21 hours (24 hpi), washed, subsampled, fixed, and replated (with 300 µL of 10X OP50-
608 1) in the same manner as described above. The plates were then incubated at 21°C for 48hours
609 (72hpi) before washing and fixing in acetone. Pulse-chase co-infection assays were performed
610 as described above, except samples were infected with either one or two species of microsporidia
611 for 24 hours total. Pulse-chase assays initiated at the L4 stage were performed by using ~3000
612 bleach-synchronized L1s mixed with 200 µL of 10X OP50-1 and plated on unseeded 6-cm NGM
613 plates for 48 hours. Worm populations were then washed two times with M9 in 1.5 mL

614 microcentrifuge tubes. 50 µL of 10X OP50-1 and spores were added to each worm population
615 and then plated on unseeded 6-cm NGM plate for 3 hours at 21°C. Samples were then
616 subsampled, washed, and replated as described above. Chitin and FISH staining were performed
617 as described above for all pulse-infection experiments.

618 ***MIP-MAP and variant analysis***

619 Wild isolates were mapped using a competitive fitness approach after crossing with males of the
620 mapping strain AWR133, a CRISPR-inserted Pmyo-2::GFP version of VC20019. Mapping was
621 completed using 2-4 competitive selection cycles on 10-cm NGM plates. Each cycle consisted of
622 2 generations of recombinant populations, each added to plates as bleach-synchronized L1
623 animals. In the first generation ~10,000 L1 cross-progeny animals were exposed to continuous
624 microsporidia infection (See **Supplementary Table S3**) for ~72 hours before bleach-
625 synchronizing. Next, ~8,000 L1s were plated within 24 hours to "rest" on 10-cm OP50-seeded
626 NGM plates and grown for ~72 hours before being bleach-synchronized. L1 progeny of the "rest"
627 phase were then plated onto both an OP50-1-seeded plate with spores to begin the next cycle
628 and a secondary plate without spores to generate a sample to collect genomic DNA. Genomic
629 samples were prepared with 250 ng of genomic DNA and VC20019 MIP-MAP library probes as
630 previously described [52]. Sequencing libraries were run on an Illumina NextSeq, with 161,054-
631 801,840 reads per library and a mean of 4005 ± 2760 reads per MIP across the entire data set.

632 **Near isogenic lines construction**

633 Near isogenic lines were tracked across chromosome I using four markers located at four
634 locations matching sequenced variants identified in JU1400: cewivar00066519 (491,763),
635 cewivar00067570 (1,051,810), cewivar00069114 (1,567,450), and cewirvar00070489
636 (2,012,869). These markers were used for restriction fragment length polymorphism analysis with
637 the enzyme DraI. JU1400 hermaphrodites were crossed with AWR133 males. F1 GFP+ animals

638 at the L4 stage were chosen to produce F2 animals. 48 GFP+ animals were chosen and screened
639 at marker cewivar00066519 for JU1400 homozygosity and further screened at cewirvar00070489
640 for JU1400 homozygosity or heterozygosity. Seven F2 lines were chosen based on their
641 genotyping and four of these gave rise to five main progenitor NILs, each of which was used to
642 create a separate GFP+ and GFP- NIL strain. In total 10 NILs were generated and tested for
643 susceptibility against LUAm1. One line was chosen for outcrossing (AWR140) which gave rise to
644 the AWR144 and AWR145 NILs.

645 ***C. elegans* Whole Genome Sequencing Analysis**

646 Worm strains used for whole genome sequencing were grown on 10-cm plates with OP50-1 for
647 3 days and allowed to starve. Plates were then washed at least two times with M9 in
648 microcentrifuge tubes before freezing in liquid freezing solution and then stored at -80C. gDNA
649 was then extracted and quantified with Qubit™ HS system. gDNA quality was determined by
650 agarose gel electrophoresis and photometric OD260/280 of 1.8-2.0. gDNA was submitted to The
651 Centre for Applied Genomics (TCAG, Hospital for Sick Children, Toronto, ON, Canada) for library
652 preparation and whole genome sequencing on an Illumina HiSeq 2500 SR50 Rapid Run flowcell
653 in pools of six samples per lane. Raw sequencing reads of each NIL were aligned to the N2
654 reference of the WBcel215 release (accession: PRJNA13758) using bowtie2 [77]. Then, samtools
655 was used to convert it into .bam format and freebayes was used to perform variant calling with
656 the default settings [78,79]. The breakpoints between VC20019 and JU1400 in chromosome I of
657 each NIL were computed and visualised using vcf-kit [80].

658 **RNA extraction and mRNA sequencing**

659 Infection samples for mRNA sequencing were prepared by mixing ~10,000 bleach-synchronized
660 L1 stage animals with 1 mL of 20X OP50-1 and 10 million *N. parisii* spores, 10 million *N. ausubeli*
661 spores, 10 million *N. ironsii* spores, and 30 million *N. ferruginous* spores in four separate

662 microcentrifuge tubes. Samples were then spread onto individual 10-cm NGM plates and allowed
663 to dry before incubating at 21°C for 48 hours. Samples for RNA extraction were washed in
664 M9/0.1% Tween-20 in 15 mL conical tubes at least three times before adding 1 mL of TRI-
665 Reagent® (Sigma-Aldrich). Total RNA extraction and ethanol precipitation protocols was
666 performed as per Tri-Reagent® manufacturers instruction. Libraries were prepared using
667 NEBNext® Ultra™ II Directional RNA Library Prep Kit for Illumina® kit as per manufacturer's
668 instruction. RNA sequencing was carried out using Illumina NovaSeq-SP flow cell by The Centre
669 for Applied Genomics (TCAG).

670 **Microsporidia RNA-seq analysis**

671 Using Bowtie2 v2.4.4, indexes were built from *Nematocida parisii* strain ERTm1 (Genbank:
672 GCF_000250985.1), *Nematocida ausubeli* strain ERTm2 (Genbank: GCA_000738915.1),
673 *Nematocida parisii* strain ERTm5 (Genbank: GCA_001642415.1) and *Nematocida ferruginous*
674 strain LUAm1 (Accession: JALPMW000000000) The genome annotation file of each *Nematocida*
675 species was converted into gtf format using Gffread v0.12.3. Paired-end reads were aligned to
676 corresponding index and genome annotation files using TopHat v2.1.2. Cufflinks v2.2.1 was used
677 to generate a transcriptome assembly for each sample, which was then combined with the
678 corresponding reference genome annotation using Cuffmerge of the Cufflinks 2.2.1 package to
679 produce a single annotation file.

680 ***C. elegans* mRNA-seq analysis**

681 The paired end reads generated for each strain were submitted as separate projects to Alaska
682 v1.7.2 (http://alaska.caltech.edu), which is an online automated RNA-seq analysis tool in
683 collaboration with Wormbase. Briefly, Bowtie2 [77], Samtools [78], RseQC [81], FastQC, and
684 MultiQC [82] were used for quality control of the input files. Kallisto [83] was used for the read
685 alignment and quantification, followed by differential analysis by Sleuth. For both N2 and JU1400

686 samples, the reads were aligned to the N2 reference of the WS268 release (accession:
687 PRJNA13758).

688 **Principal component analysis**

689 The N2 and JU1400 normalized abundance measurements generated by Alaska, were read by
690 the readRDS() function of the R package base v4.1.1. Normalized counts for each gene in each
691 strain were generated via sleuth_to_matrix() with the “obs_norm” data and “tpm” units. PCA of
692 gene expression was performed using samples from each strain, and merged samples, via the R
693 package pcaexplorer v2.20.2 [84].

694 **Differentially expressed genes of N2 and JU1400 hosts**

695 Log_2 fold change values of duplicated genes in each of the eight samples were averaged using
696 the R package dplyr v1.0.8. Genes with FDR-adjusted p-value of <0.01 were regarded as
697 significant. Significant genes expressed in at least three out of the eight samples were used for
698 hierarchical clustering via the function hclust() from the R package stats v4.1.1, then plotted using
699 R packages ggdendrogram and ggplot2 v3.3.5. Differentially upregulated genes were defined as
700 those with an FDR-adjusted p-value<0.01 and log_2 fold change >0 (infected vs. control);
701 differentially downregulated genes were defined as those with an FDR-adjusted p-value <0.01
702 and log_2 fold change <0 (infected vs. control).

703 **Strain-specific, pathogen-specific and strain-pathogen pair specific genes**

704 Strain-specific genes were defined as genes that are significantly upregulated or downregulated
705 in at least three out of the four JU1400 or N2 samples. Pathogen-specific genes were defined as
706 those significantly upregulated or downregulated in both JU1400 and N2 upon infection by the
707 same microsporidia species, but not observed when infected by other microsporidia species.
708 Moreover, strain-pathogen pair specific genes were defined as genes that are significantly

709 upregulated or downregulated in a particular strain-pathogen sample, but not observed in the
710 other seven strain-pathogen samples.

711 **Domain enrichment analysis**

712 We chose to look at F-box, MATH/BATH, PALS, DUF684 and DUF713 domains containing
713 genes, implicated from differentially regulated genes of *N. parisii* infected *C. elegans* in previous
714 publications [54,85]. Lists of gene names from respective gene classes were downloaded
715 separately from Wormbase (http://wormbase.org/) and the corresponding protein-coding
716 sequences were extracted from Wormbase ParaSite (https://parasite.wormbase.org/).
717 Alignments of other domains or classes were downloaded directly from Pfam
718 (http://pfam.xfam.org/) separately. After deleting duplicated sequences, protein sequences of
719 these classes of genes were converted to Stockholm format using Clustal Omega Multiple
720 Sequence Alignment tool (https://www.ebi.ac.uk/Tools/msa/clustalo/). Hmmbuild of HMMER
721 v3.3.2 [86] used the Stockholm format files to build respective profile HMMs, which was then
722 searched against *C. elegans* (accession: PRJNA13758) proteome of WS268 release using
723 hmmsearch. Output genes with E-value <1e-5 were used as the gene list for the enrichment
724 analyses. In the output genes, MATH and BATH genes were combined into one list; fbxa, fbxb
725 and fbxc genes were merged into the gene list for F-box (**Supplementary Table S10**). Using the
726 R package gplots v3.1.1, the number of genes overlapping between the lists and samples were
727 computed, then plotted using R package ggplot2 v3.3.5. Genes that do not fall into any of these
728 gene classes or have any of these domains were categorised as "other".

729 **Gene Set Enrichment Analysis**

730 The WormExp [56] dataset, which contains published expression data for *C. elegans*, was
731 downloaded from the WormExp v1.0 website (https://wormexp.zoologie.uni-kiel.de/wormexp/).
732 The overlap between published datasets of *C. elegans* exposed to different chemicals or

733 pathogens (**Supplementary Table S12**) and our samples, as well as the strain specific,
734 pathogen-specific, and strain-pathogen pair specific genes in our dataset were computed using
735 the R package gplots v3.1.1. For the statistical evaluation of the overlap, the p-values were
736 calculated using the adjusted Fisher exact test method from the program EASE, which removes
737 one gene in the set of intersected genes. Correction for multiple testing was implemented using
738 the Bonferroni method via the p.adjust() function in the R package stats v4.1.1.

739 **GO Biological Process, GO Molecular Function and KEGG pathway enrichment analyses**

740 Using the R package enrichR v3.0 [87], the connection to WormEnrichr, a gene list enrichment
741 analysis tool for *C. elegans*, was set through the setEnrichrSite ("WormEnrichr") function. The
742 "GO_Molecular_Function_2018", "GO_Biological_Process_2018" and "KEGG_2019" databases
743 were selected then used to query enrichr with the enrichr() function, before being plotted as
744 Enrichr GO-BP output **(Supplementary Tables S13 and S14)**.

745 **Volcano plots**

746 Values of duplicated genes in each of the four host-microsporidia samples were averaged using
747 the R package dplyr v1.0.8. Genes with FDR<0.05 and $\log_2$ Fold Change >0 or $\log_2$ Fold Changes
748 <0 were categorised as differentially upregulated or downregulated respectively. The volcano
749 plots were generated by ggplot2 v3.3.5 in R.

750 **Data and code availability**

751 All samples were deposited under NCBI BioProject PRJNA841603 and the sequence reads for
752 all samples were submitted to the NCBI Sequence Read Archive. Data from all the infection
753 experiments is in **Supplementary Data S1**. PhenoMIP analysis scripts can be found at
754 https://github.com/camok/PhenoMIP.

755

756 **Figures**

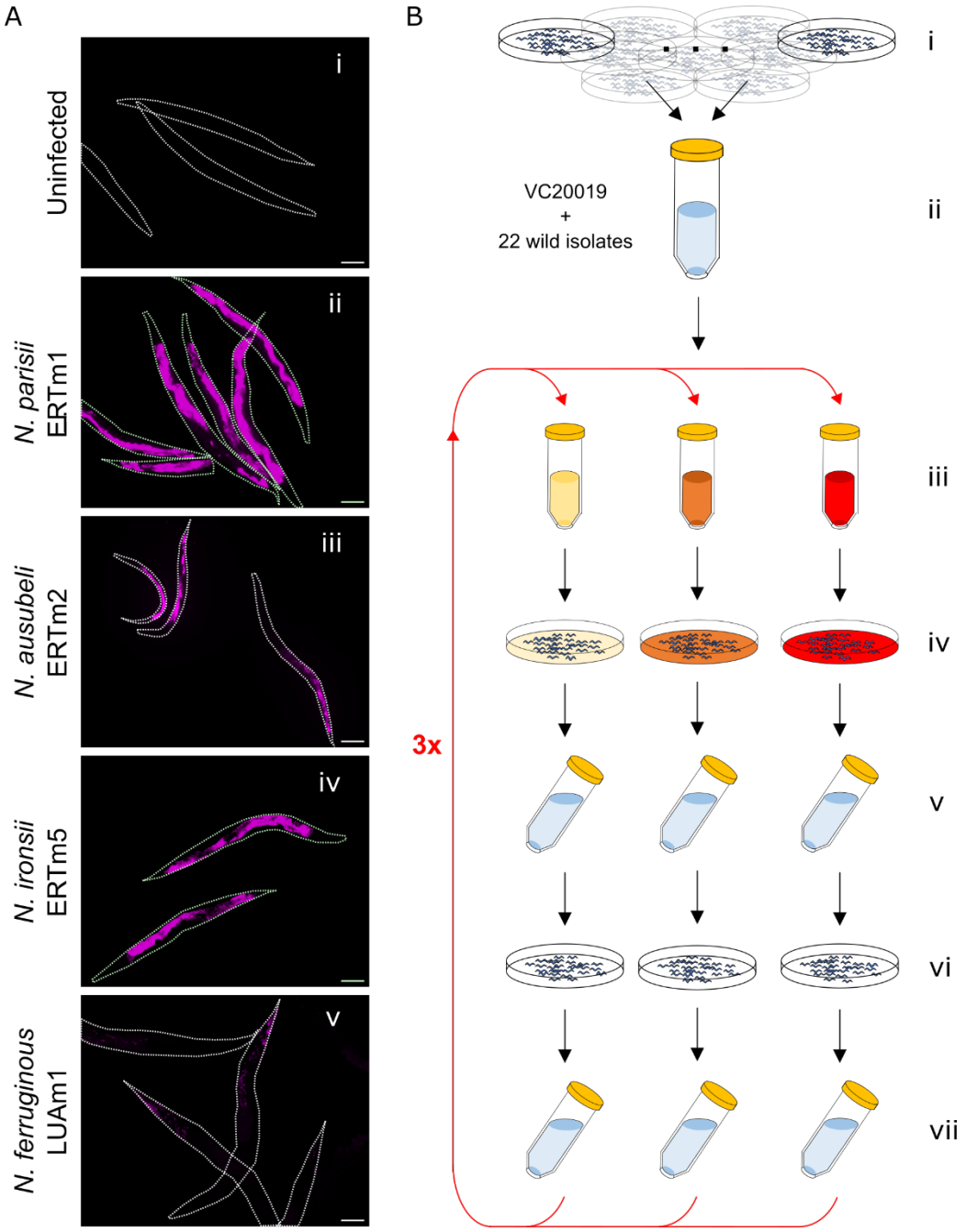

757

758 **Figure 1. A PhenoMIP high-throughput screen to identify wild strains that are either**
759 **resistant or susceptible to microsporidia infection.** (A) N2 L1 animals that were uninfected (i)
760 or exposed to either 3.5 million *N. parisii*, *N. ironsii*, or *N. ausubeli* spores or 1.25 million *N.*
761 *ferruginous* spores for 72 hours, were fixed and stained with the following 18S FISH probes (i, ii,

762 iv; MicroB-CAL Fluor Red 610, iii; Microsp1A-FAM and v; a combination of three Fluor Red 610
763 probes described in the Methods). Scale bars, 100 μm. (B) PhenoMIP screening protocol for
764 microsporidia requires that separate unstarved populations for each of the 22 wild isolate strains
765 as well as VC20019 (lab reference-derived strain) be sodium hyplochlorite-synchronized (i) before
766 pooling in equimolar amounts (ii) and infecting (iii) with different microsporidia species at doses
767 that can impose fitness challenges to the lab reference strain. Populations are grown for 72 hours
768 post-infection (iv) before sodium hypochlorite-synchronizing (v) and growing free of infection for
769 an additional 72 hours (vi). Uninfected populations are harvested, subsampled for genomic DNA,
770 and sodium hypochlorite-synchronized (vii) before repeating the infection and rest phases for an
771 additional three rounds.

772

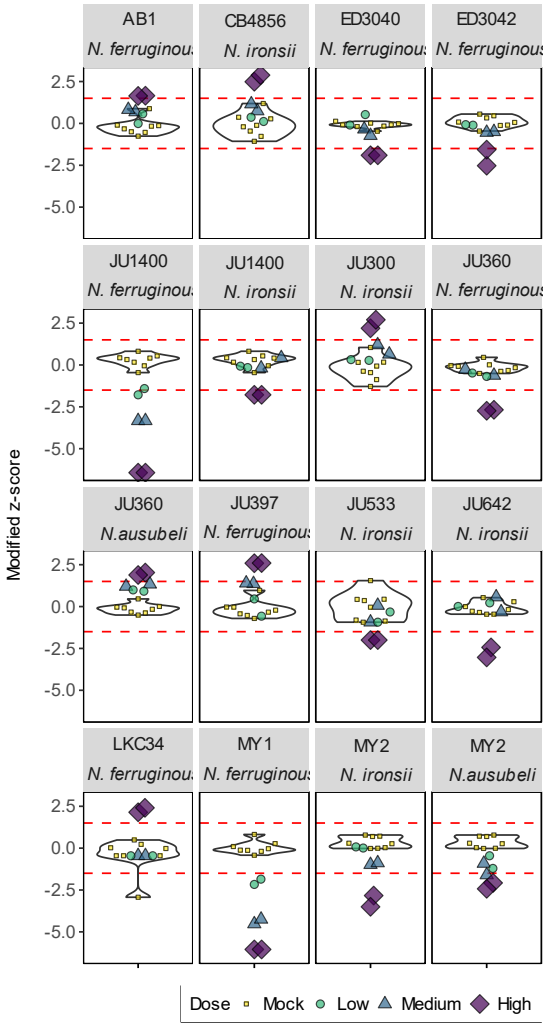

773

774 **Figure 2. Analysis of PhenoMIP mean fold-change rate identifies 16 candidate**

775 **nematode/microsporidia interactions.** Violin plots of *C. elegans* wild isolate strains infected

776 by specific microsporidia species. Violins are derived from modified z-scores of mean fold-

777 change rate (FCR) per generation using the eight mock-infection replicates of that strain.

778 Overlayed are the six infection replicates of low (green circles), medium (blue triangles), and

779 high (purple diamonds) doses for the microsporidia species indicated in each subplot title. Mock

780 infection replicates are also overlayed (yellow squares). Red dotted lines represent the

781 candidate hit threshold for modified z-scores of ±1.5.

782

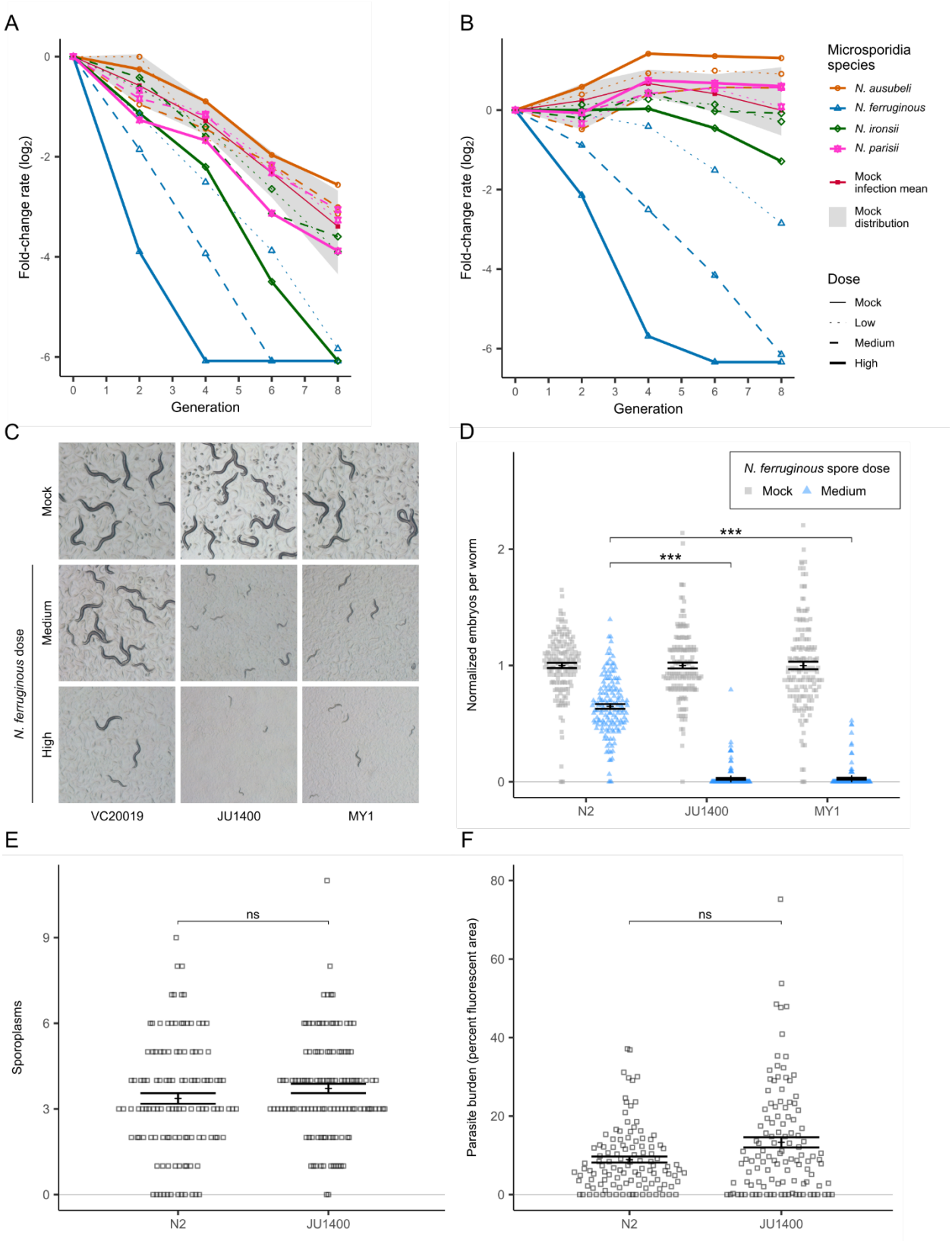
A
Fold-change rate (log2)
Generation
B
Microsporidia species
N. ausubeli
N. ferruginous
N. ironsii
N. parisii
Mock infection mean
Mock distribution
Dose
Mock
Low
Medium
High
C
Mock
N. ferruginous dose
Medium
High
VC20019
JU1400
MY1
D
N. ferruginous spore dose
Mock
Medium
Normalized embryos per worm
***
***
N2
JU1400
MY1
E
Sporoplasms
ns
N2
JU1400
F
Parasite burden (percent fluorescent area)
ns
N2
JU1400

783

784 **Figure 3. JU1400 lacks tolerance to *N. ferruginous* infection.** (A-B) Line graph of fold change
785 across multiple time points and conditions for JU1400 (A) and MY1 (B). Microsporidia strains are
786 denoted by point shape and doses of microsporidia are denoted by line type. The eight uninfected
787 control replicates are bounded within the greyed area and the mean of the uninfected control is
788 denoted by a solid red line. All other lines represent mean FCR of two biological replicate samples.
789 (C-D) Strains were infected for 72 hours with *N. ferruginous*. (C) Dissecting microscope images
790 of live animals growing on plates. (D) Dot plot of normalized embryo counts of animals fixed and
791 stained with DY96 with mean and SEM bars. Data is combined from three biological replicates
792 with n={41,50} worms per replicate sample. (E-F) N2 and JU1400 animals were infected for three
793 hours with 1.25 million spores of *N. ferruginous* before washing away uneaten spores from each
794 population. Animals were fixed after 3 hours (E) or after 72 hours (F). (E) Dot plot of sporoplasms
795 counted in N2 and JU1400 animals. Data is combined from three biological replicates with n=40
796 worms per replicate sample. (F) Bar plot with SEM bars depicting mean parasite burden as a
797 function of percent fluorescent area per animal by FISH staining in N2 and JU1400 populations.
798 Data is combined from three biological replicates with n={29, 53} worms per replicate sample. p-
799 values were determined by two-way ANOVA with Tukey post-hoc. Significance was defined as p
800 ≤ 0.001 (***) and not significant as $p > 0.05$ (ns).

801

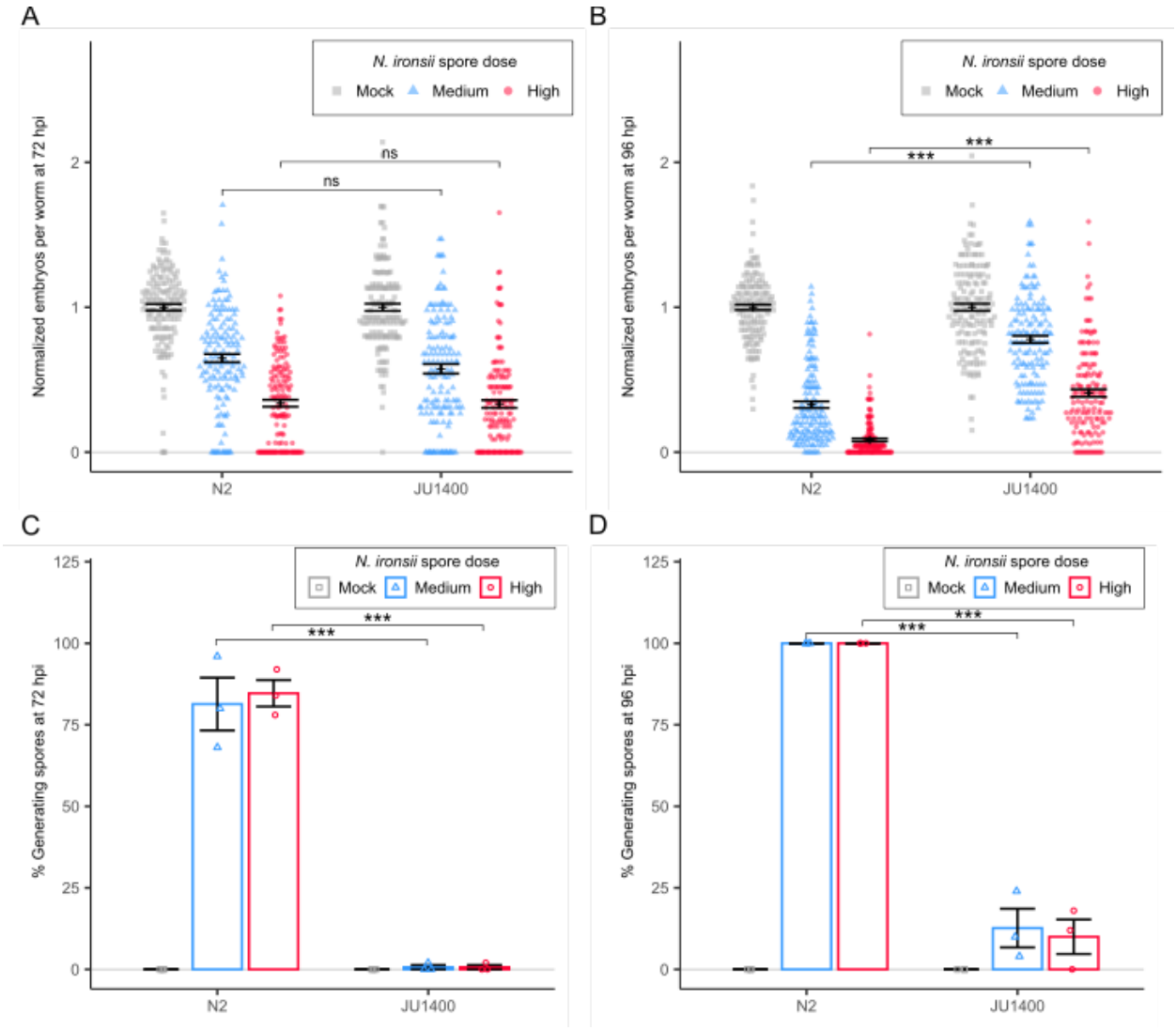

802

803 **Figure 4. JU1400 is resistant to *N. ironsii* infection.** (A-D) N2 and JU1400 were infected with
804 *N. ironsii* for 72 hours (A and C) or 96 hours (B and D), fixed, and stained with DY96. (A-B) Dot
805 plots of normalized embryo counts of animals fixed and stained with DY96 with mean and SEM
806 bars. Data is combined from three biological replicates with n={47,50} worms per replicate
807 sample. (C-D) Bar plot with SEM bars of percent population with new spore formation from three
808 combined replicate experiments. p-values were determined by two-way ANOVA with Tukey post-
809 hoc. Significance was defined as $p \leq 0.001$ (***) and not significant as $p > 0.05$ (ns).

810

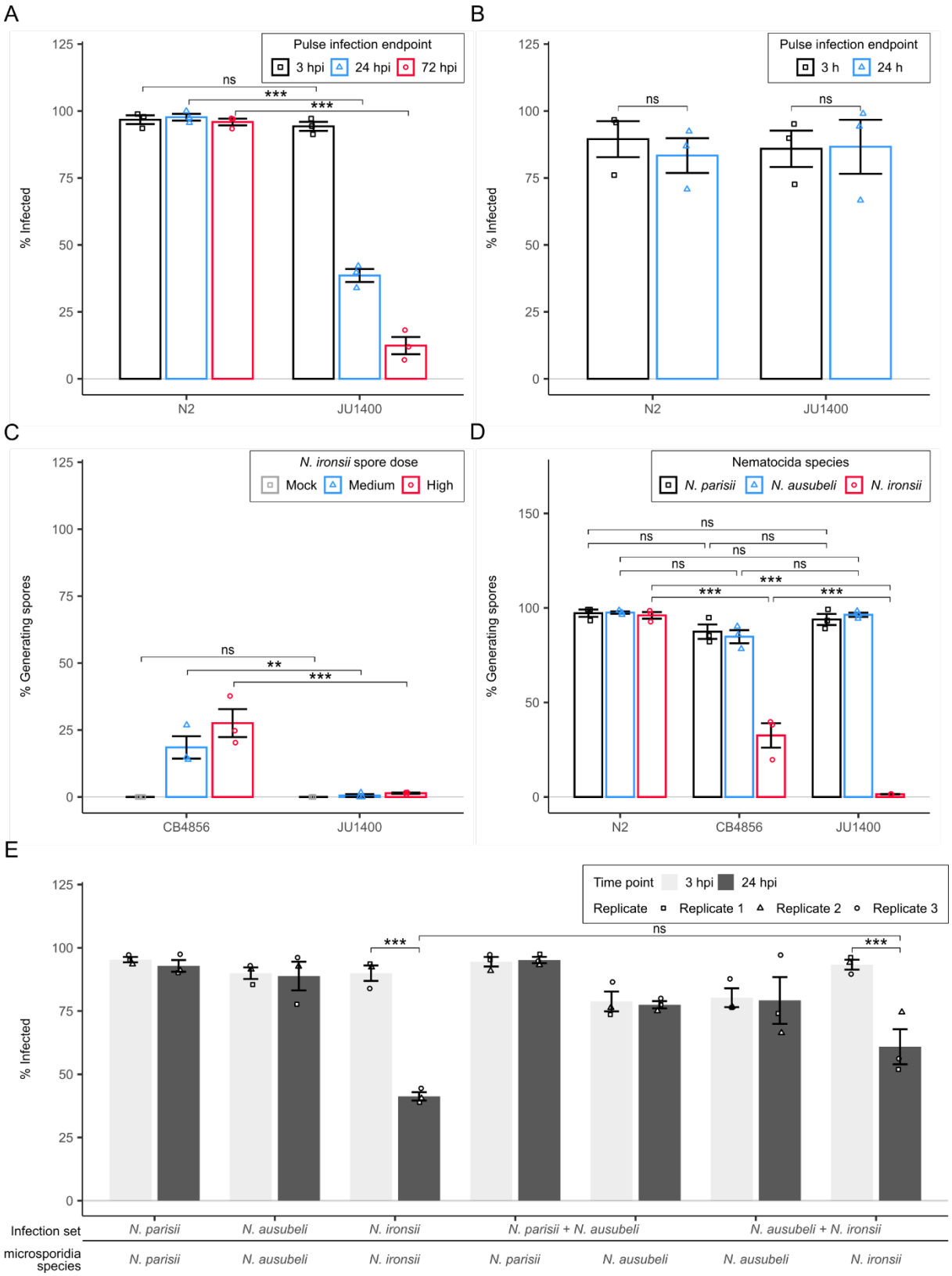
A
Pulse infection endpoint
3 hpi
24 hpi
72 hpi
% Infected
ns
***
***
N2
JU1400
B
Pulse infection endpoint
3 h
24 h
% Infected
ns
ns
N2
JU1400
C
N. ironsii spore dose
Mock
Medium
High
% Generating spores
ns
**
***
CB4856
JU1400
D
Nematocida species
N. parisii
N. ausubeli
N. ironsii
% Generating spores
ns
ns
ns
ns
ns
ns
***
***
***
N2
CB4856
JU1400
E
Time point
3 hpi
24 hpi
Replicate
Replicate 1
Replicate 2
Replicate 3
% Infected
***
ns
***
Infection set
N. parisii
N. ausubeli
N. ironsii
N. parisii + N. ausubeli
N. ausubeli + N. ironsii
microsporidia species
N. parisii
N. ausubeli
N. ironsii
N. parisii
N. ausubeli
N. ausubeli
N. ironsii

812 **Figure 5. JU1400 specifically clears *N. ironsii* infection at the earliest larval stage.** (A-B) N2
813 and JU1400 animals were pulse infected for 3 hours with *N. ironsii* before washing away excess
814 spores. Animals were pulse infected at either the L1 stage and fixed at 3-, 24-, and 72 hpi (A) or
815 animals were pulse infected at the L4 stage before fixing at 3- and 24 hpi (B). Samples were then
816 stained with an *N. parisii* 18S RNA FISH probe and animals containing either sporoplasms or
817 meronts were counted as infected. Bar plot with SEM bars show percent of animals infected per
818 replicate from three biological replicates with n=20 worms per replicate. (C) CB4856 and JU1400
819 were infected at the L1 stage with either medium or high doses of *N. ironsii* for 72 hours and then
820 fixed and stained with DY96. (D) N2, JU1400, and CB4856 were infected at the L1 stage with
821 either *N. parisii*, *N. ausubeli*, or *N. ironsii* for 72 hours and then fixed and stained with DY96. (C-
822 D) Bar plot with SEM bars show percent of animals generating spores per replicate from three
823 biological replicates with n=20 worms per replicate. (E) JU1400 animals were pulse infected for 3
824 hours with *N. parisii*, *N. ausubeli*, *N. ironsii, N. parisii* + *N. ausubeli, or N. ausubeli* + *N. ironsii*
825 before washing away excess spores. Animals were either fixed immediately at 3 hpi or at 24 hpi.
826 Samples were then stained with species-specific 18S rRNA FISH probes and animals containing
827 either sporoplasms or meronts were counted as infected. Bar plot with SEM bars show percent
828 of animals infected per replicate from three biological replicates with n={78, 147} worms per
829 replicate. p-values were determined by two-way ANOVA with Tukey post-hoc. Significance was
830 defined as $p \leq 0.01$ (**), $p \leq 0.001$ (***), and not significant as $p > 0.05$ (ns).

831

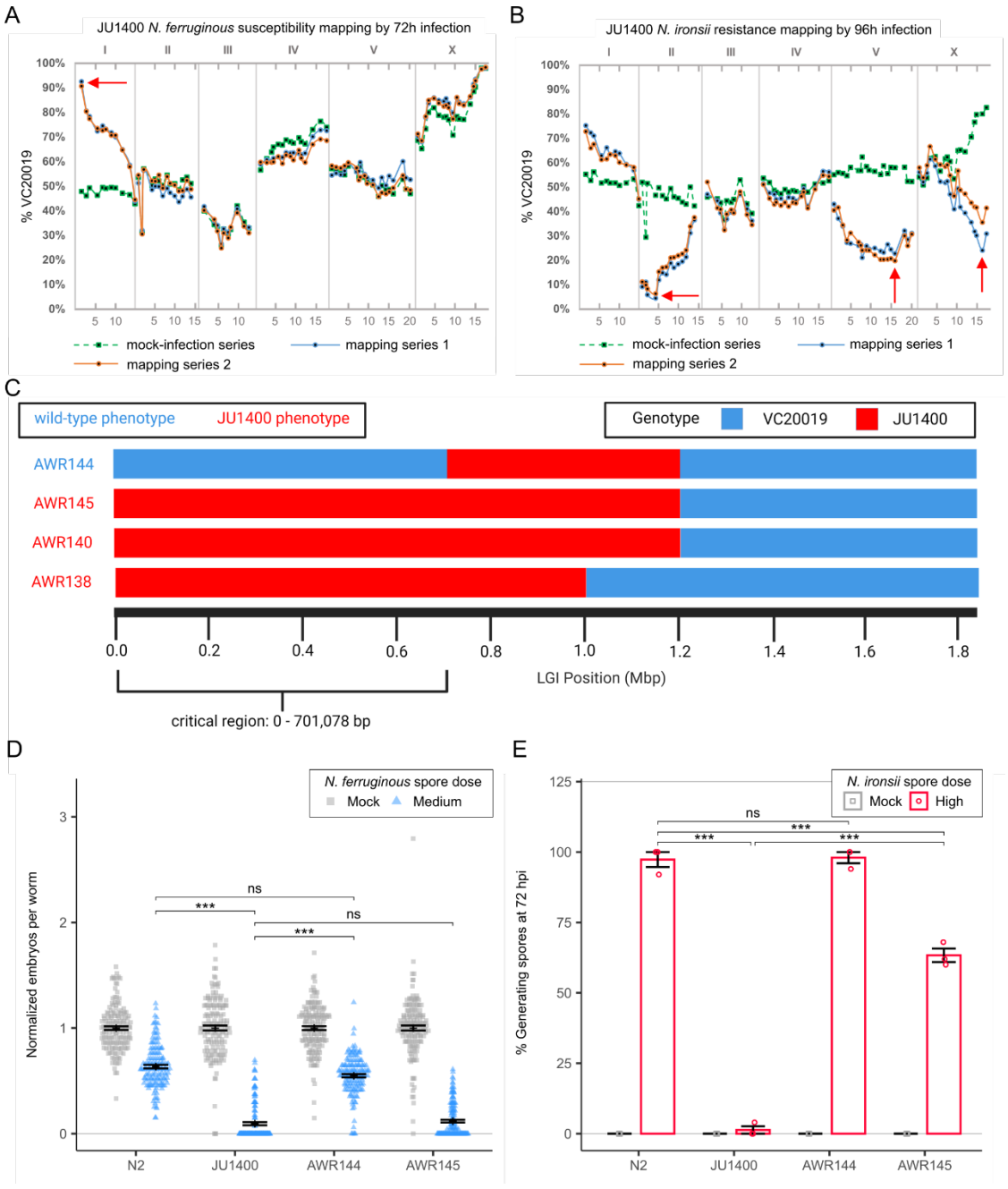

Figure 6. Genetic mapping of JU1400 host-response phenotypes identifies distinct loci. Genetic mapping of JU1400 susceptibility to *N. ferruginous* (A) and JU1400 resistance to *N. ironsii* (B) was performed with MIP-MAP using the AWR133 mapping strain. Green square-points and dotted lines represent a mock-infection replicate with the solid blue and orange lines representing two biological replicates exposed to specific infection conditions. Red arrows indicate candidate

838 regions of interest based on the expected genome fixation direction during phenotype selection.
839 (C) Whole-genome sequencing haplotype map of chromosome I NILs generated from crosses
840 between JU1400 and AWR133. Regions of chromosome I for specific NILs are coloured by their
841 inferred haplotype. Strain names are indicated to the left of each with AWR138, AWR140, and
842 AWR145 sharing a susceptibility phenotype (Red text) while AWR144 is not susceptible (Blue
843 text) to *N. ferruginous* infection. (D) N2, JU1400, AWR144, and AWR145 L1 stage animals were
844 infected with *N. ferruginous* before being fixed at 72 hpi and stained with DY96 to visualize
845 embryos. Dot plot of normalized embryo counts of with mean and SEM bars. Data is combined
846 from three biological replicates with n=50 worms per replicate sample. (E) N2, JU1400, AWR144,
847 and AWR145 L1 stage animals were infected with *N. ironsii* before being fixed at 72 hpi and
848 stained with DY96 to visualize mature spores. Bar plot with SEM bars show percent of animals
849 generating new spores per replicate from three biological replicates with n=50 worms per
850 replicate. p-values were determined by two-way ANOVA with Tukey post-hoc. Significance was
851 defined as $p \leq 0.001$ (***) and not significant as $p > 0.05$ (ns).

852

853

854

855

856

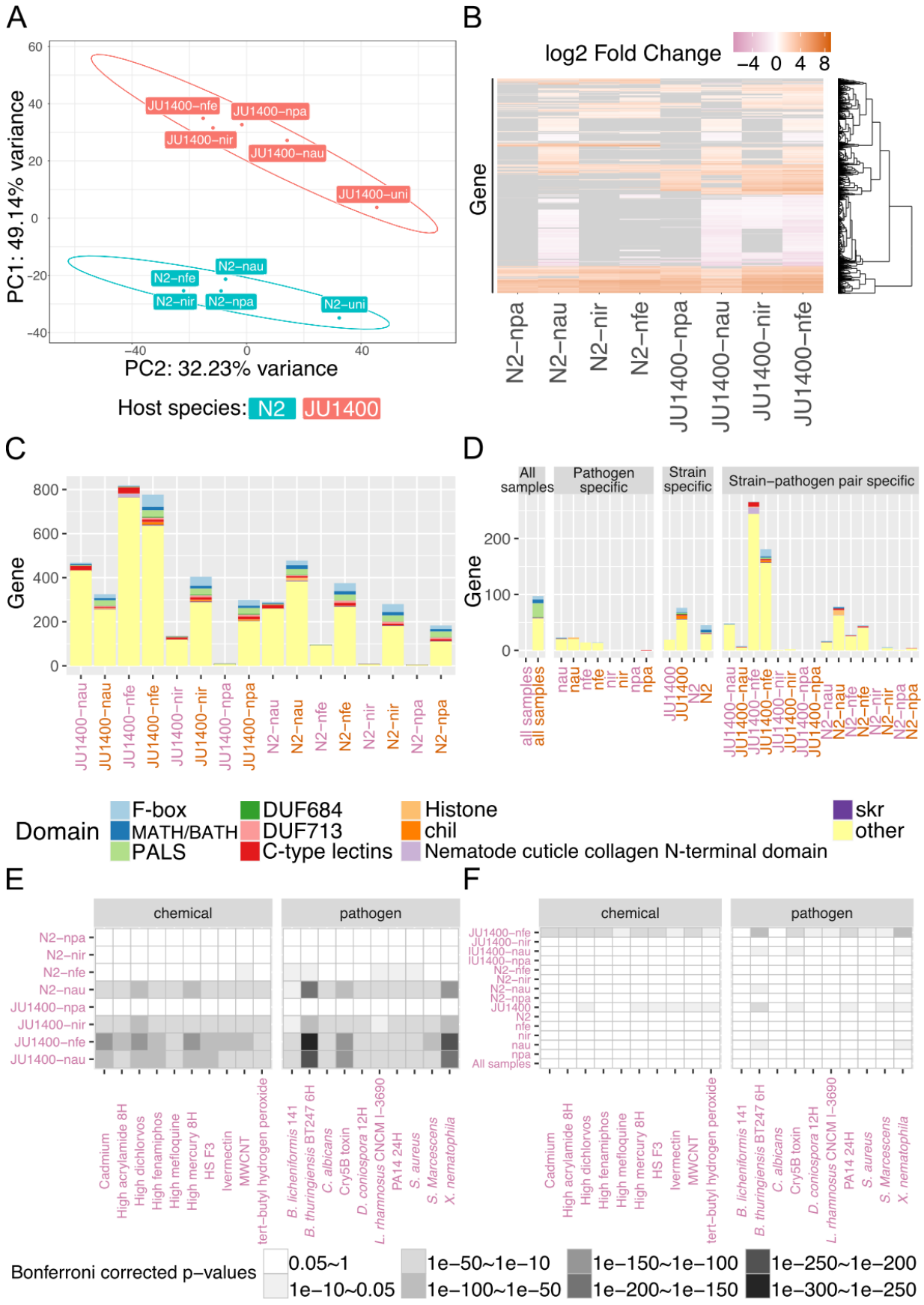
A
PC1: 49.14% variance
PC2: 32.23% variance
JU1400−nfe
JU1400−npa
JU1400−nir
JU1400−nau
JU1400−uni
N2−nau
N2−nfe
N2−nir
N2−npa
N2−uni
Host species: N2 JU1400
B
log2 Fold Change
−4 0 4 8
Gene
N2−npa
N2−nau
N2−nir
N2−nfe
JU1400−npa
JU1400−nau
JU1400−nir
JU1400−nfe
C
Gene
D
All samples
Pathogen specific
Strain specific
Strain−pathogen pair specific
Domain
F-box
MATH/BATH
PALS
DUF684
DUF713
C-type lectins
Histone
chil
Nematode cuticle collagen N-terminal domain
skr
other
E
chemical
pathogen
Cadmium
High acrylamide 8H
High dichlorvos
High fenamiphos
High mefloquine
High mercury 8H
HS F3
Ivermectin
MWCNT
tert−butyl hydrogen peroxide
B. licheniformis 141
B. thuringiensis BT247 6H
C. albicans
Cry5B toxin
D. coniospora 12H
L. rhamnosus CNCM I−3690
PA14 24H
S. aureus
S. Marcescens
X. nematophila
F
Bonferroni corrected p−values
0.05~1
1e−10~0.05
1e−50~1e−10
1e−100~1e−50
1e−150~1e−100
1e−200~1e−150
1e−250~1e−200
1e−300~1e−250

857

858 **Figure 7. RNA-seq analysis of N2 and JU1400 infected with four species of microsporidia.**
859 N2 and JU1400 animals were infected with one of four species of microsporidia (see Methods for
860 doses) for 48 hours and RNA was extracted and sequenced. (A) Principal component analysis of
861 uninfected and infected N2 and JU1400 samples. Circles represent confidence ellipses around
862 each strain at 95% confidence interval. (B) Heatmap of transcriptional profiles of differentially
863 regulated genes in N2 and JU1400 samples. Rows represent genes clustered hierarchically.
864 Scale is of differential regulation of infected compared to uninfected samples. Grey tile indicates
865 that the gene is not significantly differentially regulated in the sample. (C-D) Domain enrichment
866 analysis of significantly upregulated and downregulated genes in each sample (C) and of specific
867 gene sets (strain, pathogen, and strain-pathogen pair) (D). (E-F) Published datasets of
868 differentially expressed *C. elegans* genes upon exposure to chemicals or bacterial infection were
869 compared for overlap with the downregulated genes from each sample (E) or for overlap between
870 of differentially expressed genes in strain specific, pathogen specific, or strain-pathogen sets (F).
871 (A-F) uni (uninfected), npa (*N. parisii)*, nau (*N. ausubeli*), nir (*N. ironsii),* and nfe (*N. ferruginous)*.
872 Upregulated samples are represented with orange text; downregulated samples are represented
873 with pink text.

874

875

876

877

878

879

880

881

882 **Supplementary material**

883 **Figure S1. Geographical locations of *C. elegans* and microsporidia used in this study.**

884 **Figure S2. Analysis of PhenoMIP mean fold-change rate identifies candidate**
885 **nematode/microsporidia interactions.**

886 **Figure S3. The Hawaiian (CB4856) strain shows resistance to infection by high-dose *N.***
887 ***ironsii*.**

888 **Figure S4. Single-strain testing of PhenoMIP interaction candidates with *N. ferruginous***
889 **infection.**

890 **Figure S5. Single-strain testing of PhenoMIP interaction candidates with *N. ironsii***
891 **infection.**

892 **Figure S6. Single-strain testing of PhenoMIP interaction candidates with *N. ausubeli***
893 **infection.**

894 **Figure S7. JU1400 and MY1 share similar response phenotypes to infection by *N.***
895 ***ferruginous*.**

896 **Figure S8. JU1400 and N2 display similar levels of *N. ferruginous* infection.**

897 **Figure S9. JU1400 displays a similar response to *N. ferruginous* strains and sensitivity to**
898 ***N. cider*.**

899 **Figure S10. JU1400 is resistant to infection by *N. ironsii*.**

900 **Figure S11. JU1400, but not N2, can specifically eliminate *N. ironsii* infection.**

901 **Figure S12. Genetic mapping of CB4856 resistance to *N. ironsii.***

902 **Figure S13. Genetic mapping of interaction phenotypes of JU1400 to *N. ironsii* and MY1 to**
903 ***N. ferruginous* using 72-hour selections.**

904 **Figure S14. JU1400 and MY1 susceptibility to *N. ferruginous* is recessive and MY1 is less**
905 **resistant than JU1400 to *N. ironsii*.**

906 **Figure S15. Generation of NILs carrying the chromosome I region that is responsible for**
907 **susceptibility to *N. ferruginous*.**

908 **Figure S16. Microsporidia mRNA reads per sample demonstrates JU1400 resistance to *N.***
909 ***ironsii*.**

910 **Figure S17. Principal component analysis of N2 and JU1400 samples.**

911 **Figure S18. Comparison of correlation between N2 and JU1400 strains after infection with**
912 **different microsporidia species.**

913 **Figure S19. Volcano plots of differentially regulated genes.**

914 **Figure S20. Overlap between the significant upregulated genes upon microsporidia**
915 **infection and differentially expressed datasets of *C. elegans* genes upon exposure to**
916 **chemicals or bacterial infection.**

917 **Table S1. Microsporidia species information.**

918 **Table S2. PhenoMIP microsporidia infection doses.**

919 **Table S3. Wild isolate mapping microsporidia infection doses.**

920 **Table S4. NIL strain chromosome I region composition.**

921 **Table S5. Candidate genes found in chromosome I region for *N. ferruginous* sensitivity.**

922 **Table S6. Microsporidia gene FPKM values in N2 and JU1400.**

923 **Table S7: Normalized *C. elegans* gene counts for all RNA-seq replicates from this study.**

924 **Table S8: Results of *C. elegans* differential expression analyses for all RNA-seq**
925 **comparisons performed in this study.**

926 **Table S9. Gene classes and domains used for enrichment analyses.**

927 **Table S10. The number of differentially regulated genes that contain enriched domains.**

928 **Table S11. Published data sets from WormExp used in this study.**

929 **Table S12. List of gene set overlaps from this study to published data sets.**

930 **Table S13. GO Biological Processes, GO Molecular Functions, and KEGG Pathways**
931 **enriched in N2 genes upregulated or downregulated upon microsporidia infection.**

932 **Table S14. GO Biological Processes, GO Molecular Functions, and KEGG Pathways**
933 **enriched in JU1400 genes upregulated or downregulated upon microsporidia infection.**

934 **Data S1. Data of all infection experiments.**

935

A

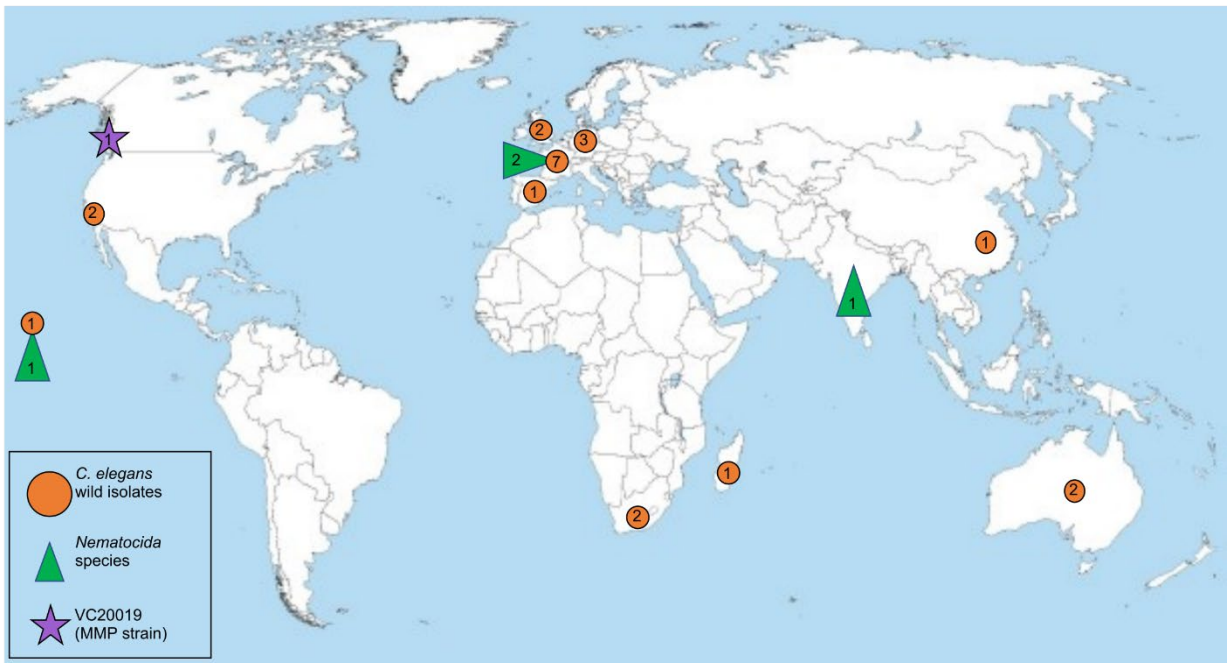

936

937 **Figure S1. Geographical locations of *C. elegans* and microsporidia used in this study.** (A)
938 World map highlighting the locations where the *C. elegans* wild isolate strains (orange circles),
939 *Nematocida* species (green triangles), and the VC20019 reference strain (purple star) used in this
940 study were originally isolated.

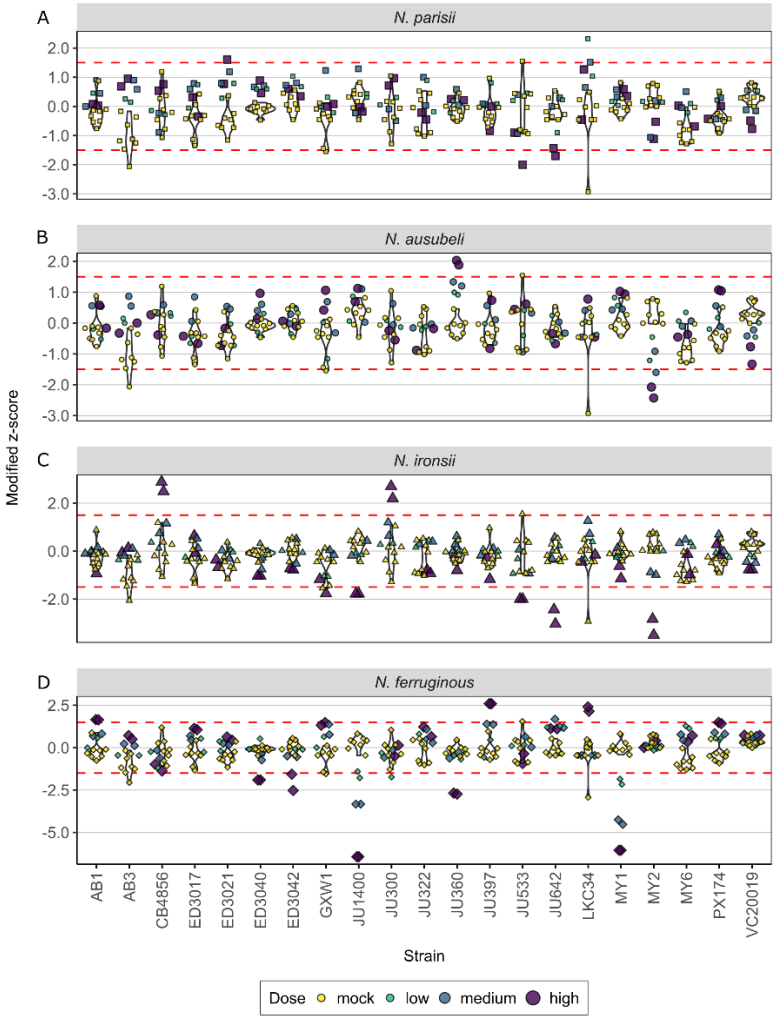

941

942 **Figure S2. Analysis of PhenoMIP mean fold-change rate identifies candidate**
943 **nematode/microsporidia interactions.** Violin plots of 20 wild isolates and lab reference-derived
944 control strain VC20019 showing modified z-scores of mean fold-change rate (FCR) per
945 generation. Violin shapes are derived from the eight mock-infection replicates. Overlayed are the
946 eight mock infections replicates and six infection replicates for each of *N. parisii* (A), *N. ausubeli*
947 (B), *N. ironsii* (C), and *N. ferruginous* (D). Replicates are coloured by mock infection (yellow), low
948 dose (green), medium dose (blue), and high dose (purple) with increasing point size associated
949 with increasing dose. Dotted lines represent the z-score candidate threshold of ±1.5. The strains
950 CB4854 and JU312 were excluded from analysis due to low initial population abundance.

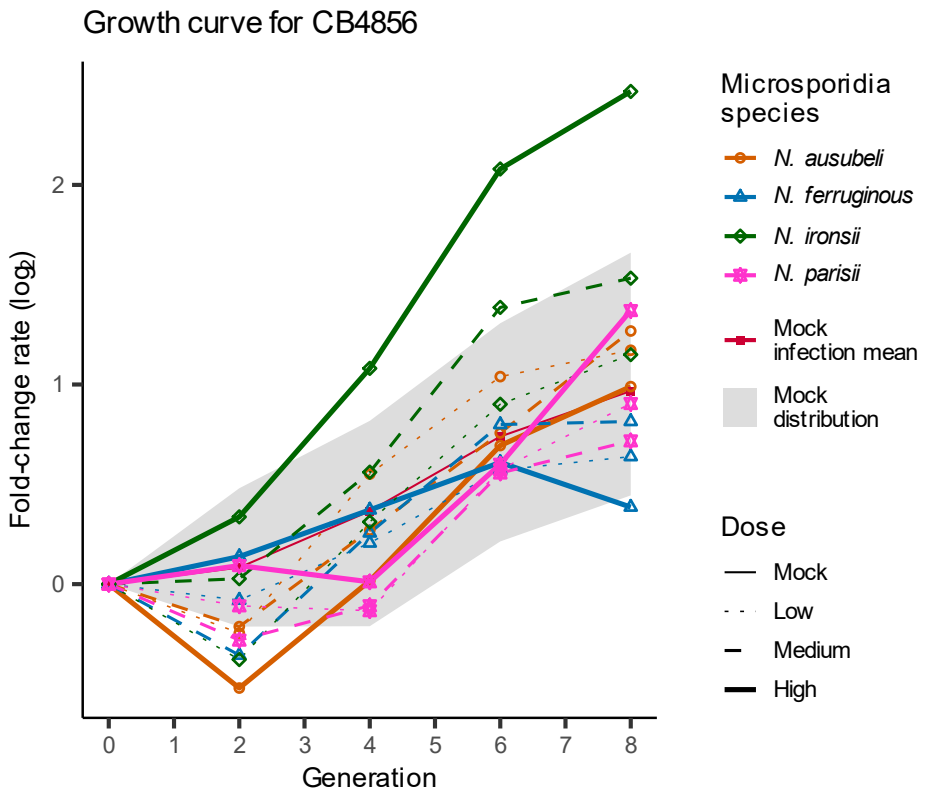

Figure S3. The Hawaiian (CB4856) strain shows resistance to infection by high-dose *N. ironsii*. Line graph of fold change across multiple time points and conditions for CB4856 demonstrates potential fitness increase relative to mock-infection conditions when infected with a high dose of *N. ironsii*. Microsporidia strains are denoted by point shape and doses of microsporidia are denoted by line type. The eight uninfected control replicates are bounded within the greyed area with the mean of the uninfected controls denoted by a solid red line. All other lines represent mean FCR of two biological replicate samples.

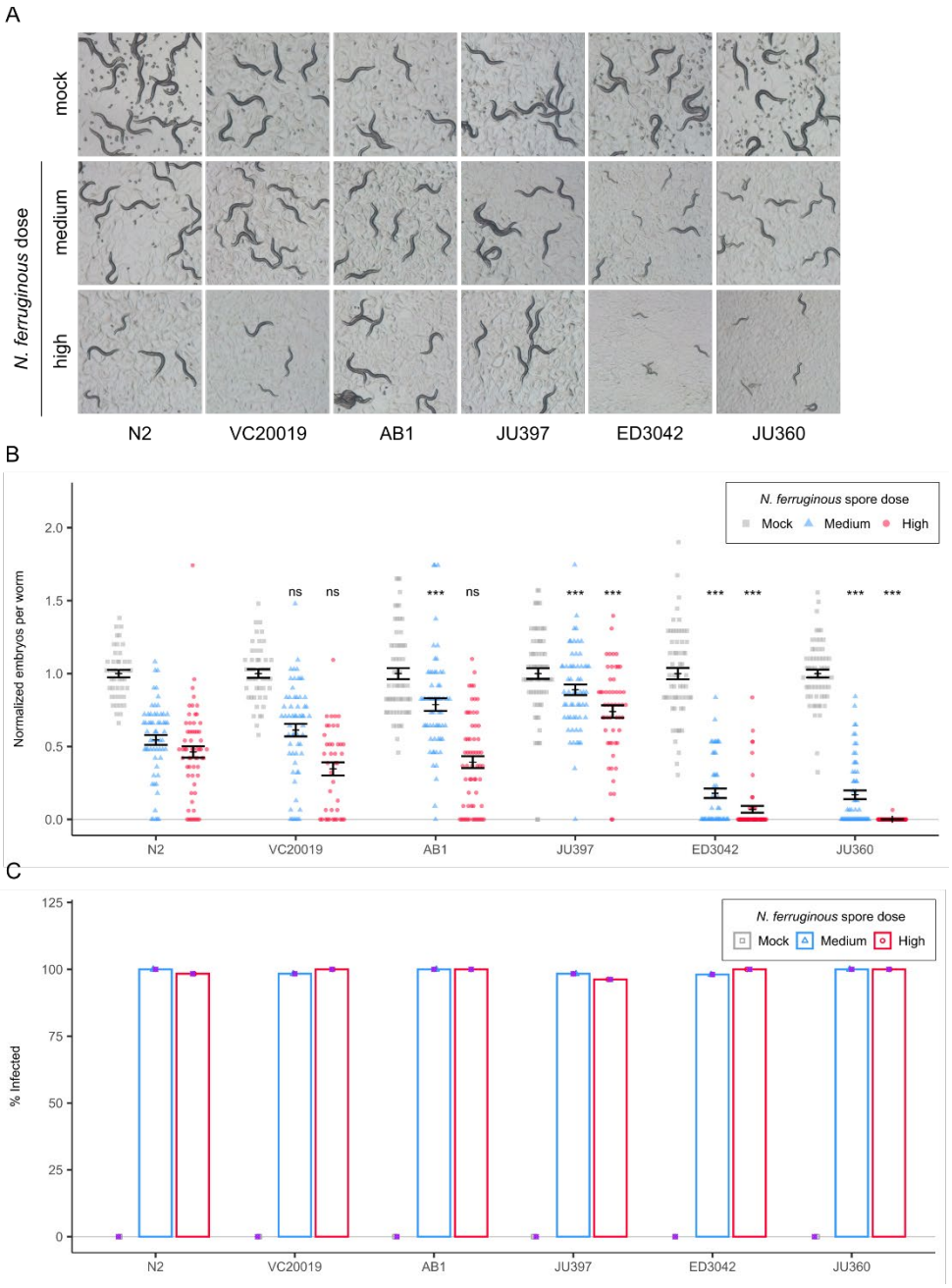

Figure S4. Single-strain testing of PhenoMIP interaction candidates with *N. ferruginous* infection. (A-C) Strains of *C. elegans* were infected with medium and high doses of *N. ferruginous* for 72 hours, imaged, fixed, and stained with DY96 and a *N. ferruginous* 18S rRNA FISH probe. (A) images of N2 and VC20019 controls versus AB1, JU397, ED3042, and JU360 at 72 hpi. (B) Dot plot with mean and SEM bars of normalized embryo counts from infected populations with n={41,70} worms per sample. (C) Bar plot depicting the percent of animals with detectable meront

967 staining. p-values denote comparison to N2 controls and were determined by two-way ANOVA
968 with Tukey post-hoc. Significance was defined as $p \leq 0.001$ (***) and not significant as $p > 0.05$
969 (ns).

970

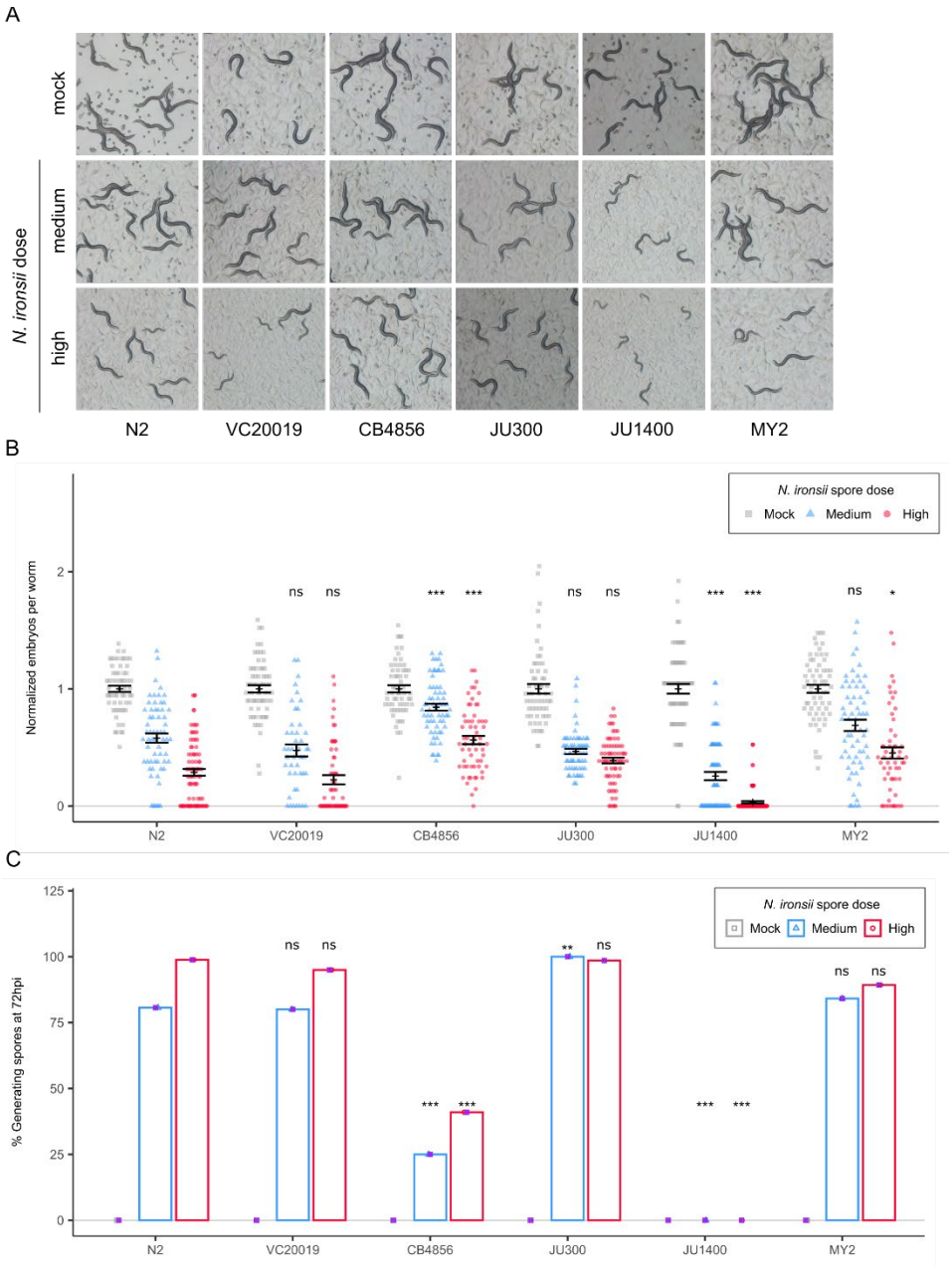

971

972 **Figure S5. Single-strain testing of PhenoMIP interaction candidates with *N. ironsii***
973 **infection.** (A-C) Strains of *C. elegans* were infected with medium and high doses of *N. ironsii* for
974 72 hours, imaged, fixed, and stained with DY96. (A) images of N2 and VC20019 controls versus
975 CB4856, JU300, JU1400, and MY2 at 72 hpi. (B) Dot plot with mean and SEM bars of normalized
976 embryo counts from infected populations with n={45,115} worms per sample. (C) Bar plot
977 depicting the percent of animals with newly generated spores. p-values denote comparison to N2

978 controls and were determined by two-way ANOVA with Tukey post-hoc. Significance was defined

979 as $p \leq 0.001$ (***), $p \leq 0.01$ (**), $p \leq 0.05$ (*) and not significant as $p > 0.05$ (ns).

980

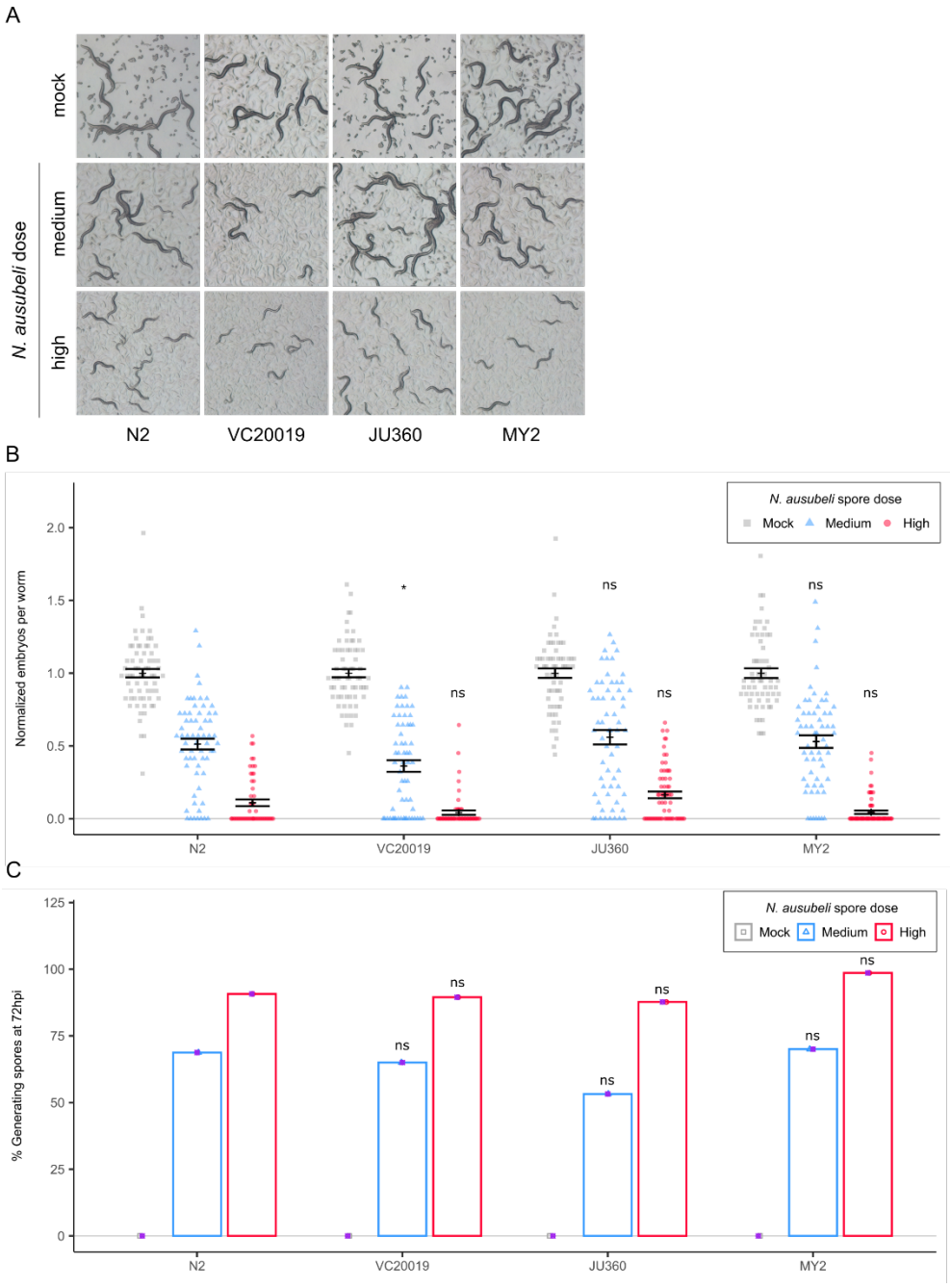

981

982 **Figure S6. Single-strain testing of PhenoMIP interaction candidates with *N. ausubeli***
983 **infection.** (A-C) Strains of *C. elegans* were infected with medium and high doses of *N. ausubeli*
984 for 72 hours, imaged, fixed, and stained with DY96. (A) images of N2 and VC20019 controls
985 versus JU360 and MY2 at 72 hpi. (B) Dot plot with mean and SEM bars of normalized embryo
986 counts from infected populations with n={54,71} worms per sample. (C) Bar plot depicting the

987 percent of animals with newly generated spores. p-values denote comparison to N2 controls and
988 were determined by two-way ANOVA with Tukey post-hoc. Significance was defined as $p \leq 0.05$
989 (*) and not significant as $p > 0.05$ (ns).

990

991

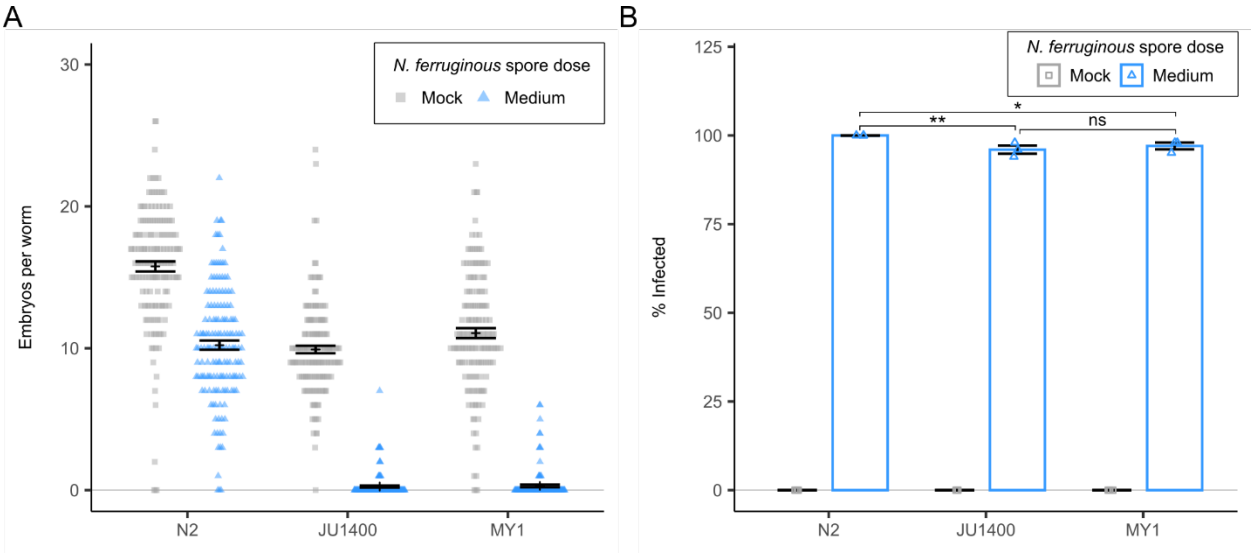

992

993 **Figure S7. JU1400 and MY1 share similar response phenotypes to infection by *N.***
994 ***ferruginous*.** JU1400, MY1, and N2 L1s were infected with a medium dose of *N. ferruginous* for
995 72 hours, fixed, and stained with *N. ferruginous* 18S rRNA FISH probes and DY96. (A) Dot plot
996 with mean and SEM bars of embryo counts from infected populations. (B) Bar plot with SEM bars
997 depicting the percent of animals with visible meronts by FISH staining. Data is combined from
998 three biological replicates with n={41,50} worms per replicate sample. p-values denote
999 comparison to N2 controls and were determined by two-way ANOVA with Tukey post-hoc.
1000 Significance was defined as $p \leq 0.01$ (**), $p \leq 0.05$ (*) and not significant as $p > 0.05$ (ns).

1001

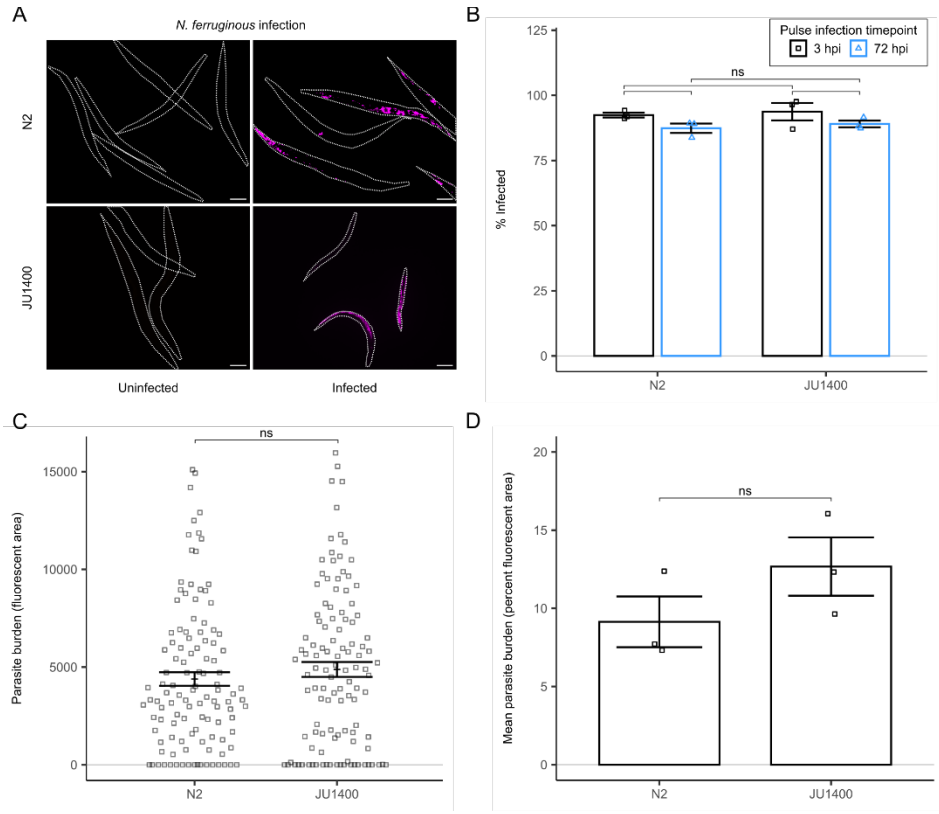

Figure S8. JU1400 and N2 display similar levels of *N. ferruginous* infection. (A-D) JU1400 and N2 L1s were infected with 1.25 million spores of *N. ferruginous* for 3 h, washed to remove spores, and replated for an additional 69 h. Animals were fixed at 3 hpi and 72 hpi and stained with *N. ferruginous* 18S rRNA FISH probes. (A) Representative images of infected animals at 72 hpi. Scale bars are 100 µm. (B) Bar plot with SEM bars depicting the percent of animals displaying either sporoplasm (3 hpi) or meronts (72 hpi) by FISH staining. (C-D) quantitation of FISH stain at 72 hpi. (C) Dot plot with mean and SEM bars of parasite burden by area in infected populations with a minimum of n={41,50} worms per sample. (D) Bar plot with SEM bars depicting mean parasite burden as a function of percent fluorescent area per animal by FISH staining. Data in (C, D) is combined from three biological replicates with n=40 worms per replicate sample. p-values denote comparison to N2 or JU1400 controls and were determined by two-way ANOVA with Tukey post-hoc. Not significant was defined as $p > 0.05$ (ns).

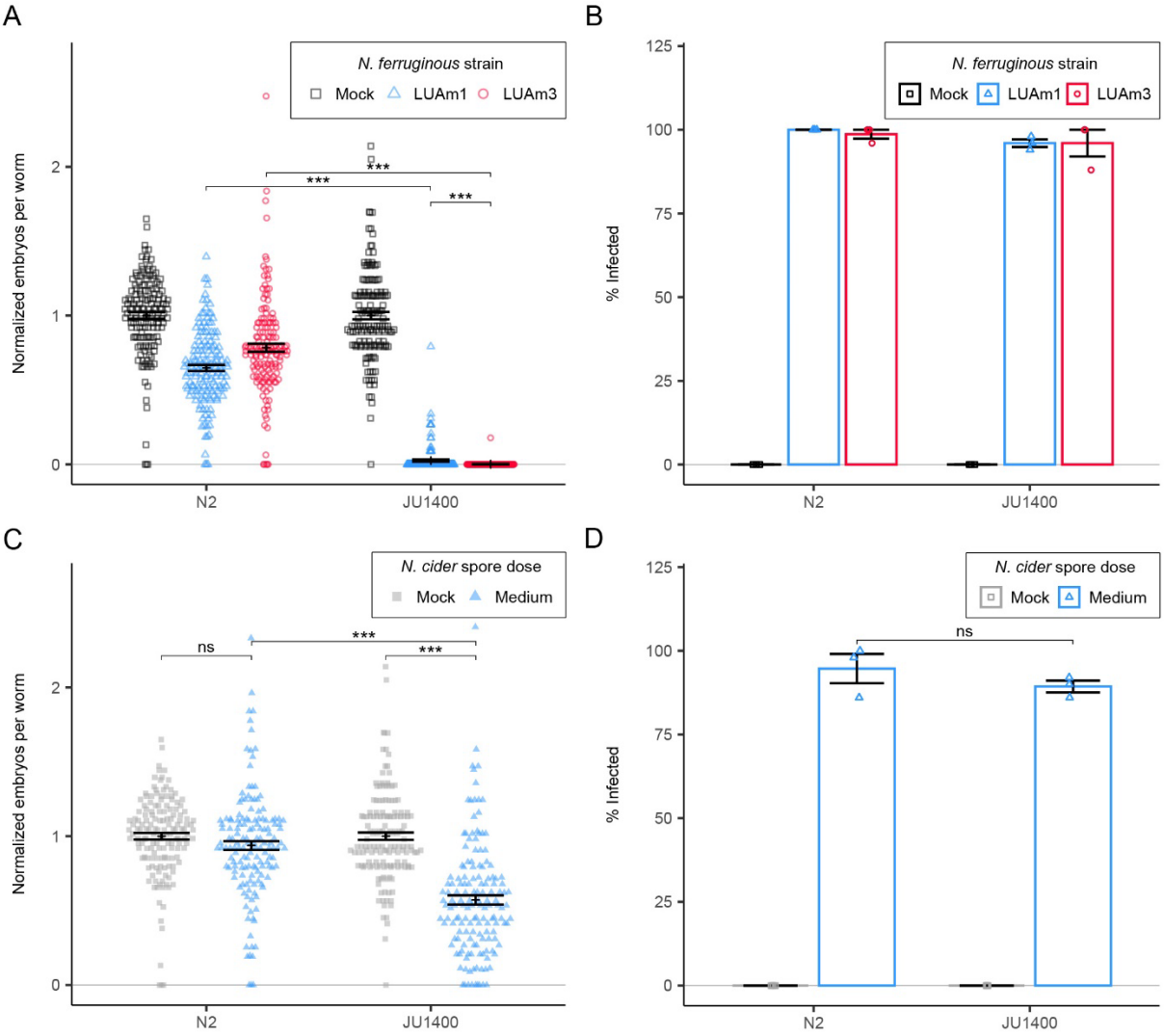

1016

1017 **Figure S9. JU1400 displays a similar response to *N. ferruginous* strains and sensitivity to**
1018 ***N. cider*.** (A-D) N2 and JU1400 L1 stage animals were infected with medium doses of *N.*
1019 *ferruginous* strain LUAm1 or LUAm3 (A-B) or a medium dose of *N. cider* (C-D) for 72 hours, fixed,
1020 and stained with DY96 and 18S rRNA FISH probe. (A, C) Dot plot of normalized embryo counts
1021 of animals with mean and SEM bars. (B, D) Bar plot with SEM bars of percent population with
1022 meronts visible. Data are combined from three biological replicates with n=50 worms per replicate.
1023 p-values were determined by two-way ANOVA with Tukey post-hoc. Significance was defined as
1024 $p \leq 0.05$ (*), $p \leq 0.001$ (***), and not significant as $p > 0.05$ (ns).

1025

1026

1027

1028

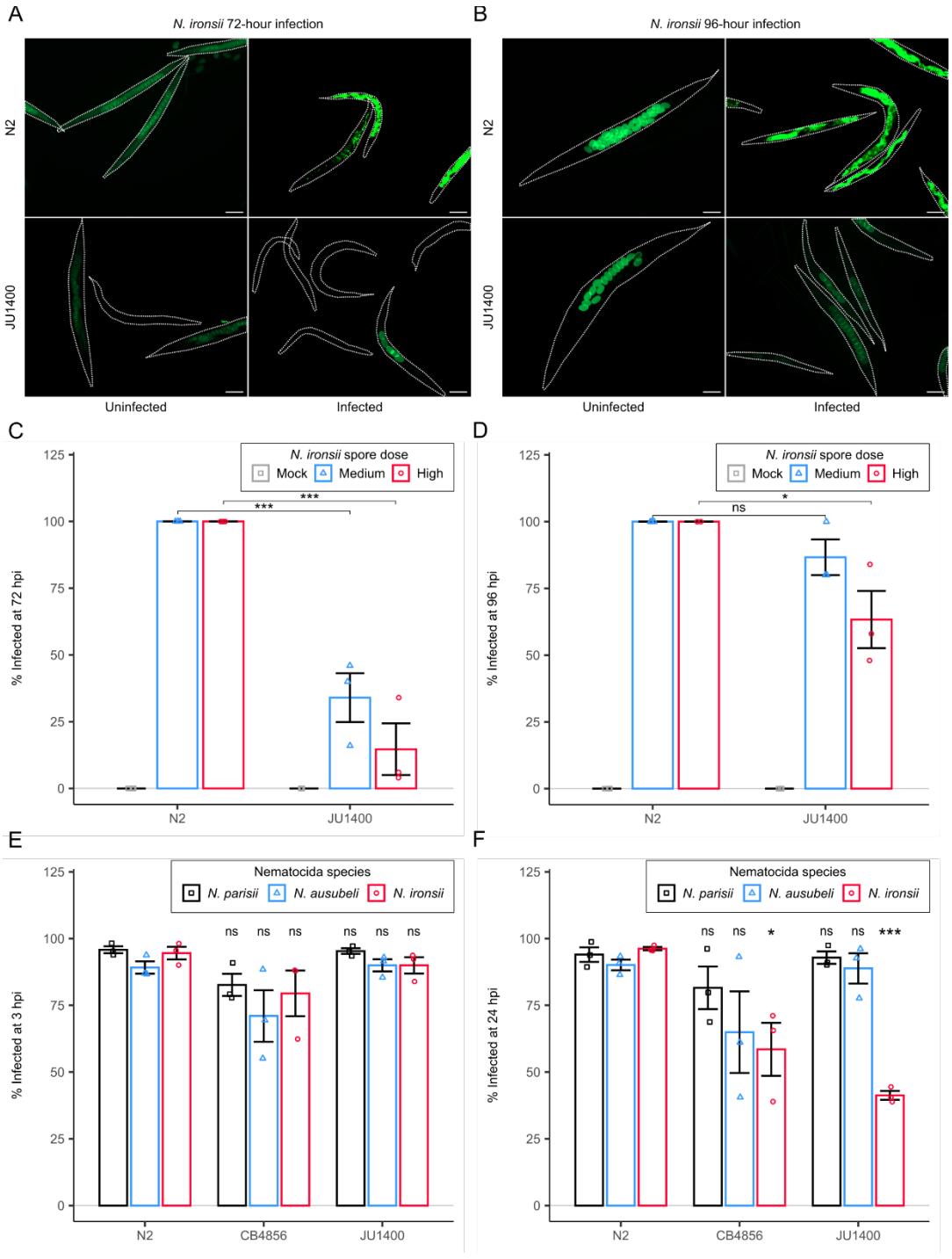

Figure S10. JU1400 is resistant to infection by *N. ironsii*. N2 and JU1400 L1 stage animals were infected with mock, medium, and high doses of *N. ironsii* for 72 (A and C) and 96 (B and D) hours and fixed. Embryos and mature spores are visualized by staining with DY96 (green), meronts are stained by a 18S rRNA FISH probe. (A-B) Representative images of high dose

1034 infection from each experiment. Scale bars are 100 μm. (C-D) Bar plots with SEM bars of percent
1035 population with meronts visible. Data in (C, D) is combined from three biological replicates each
1036 with n={47,50} worms per replicate. (E-F) N2, JU1400, and CB4856 animals at the L1 stage were
1037 infected for 3 hours with 1.25 million spores of either *N. parisii*, *N. ausubeli*, or *N. ironsii* before
1038 washing away excess spores. Animals were either fixed at 3 hours (E) or replated for an additional
1039 21 hours (F) and then fixed. Shown are bar plots with SEM bars of percent population with
1040 meronts visible. Data in (E, F) are combined from three biological replicates each with n={59,179}
1041 worms per replicate. p-values were determined by two-way ANOVA with Tukey post-hoc.
1042 Significance was defined as $p \leq 0.05$ (*), $p \leq 0.001$ (***), and not significant as $p > 0.05$ (ns).

1043

1044

1045

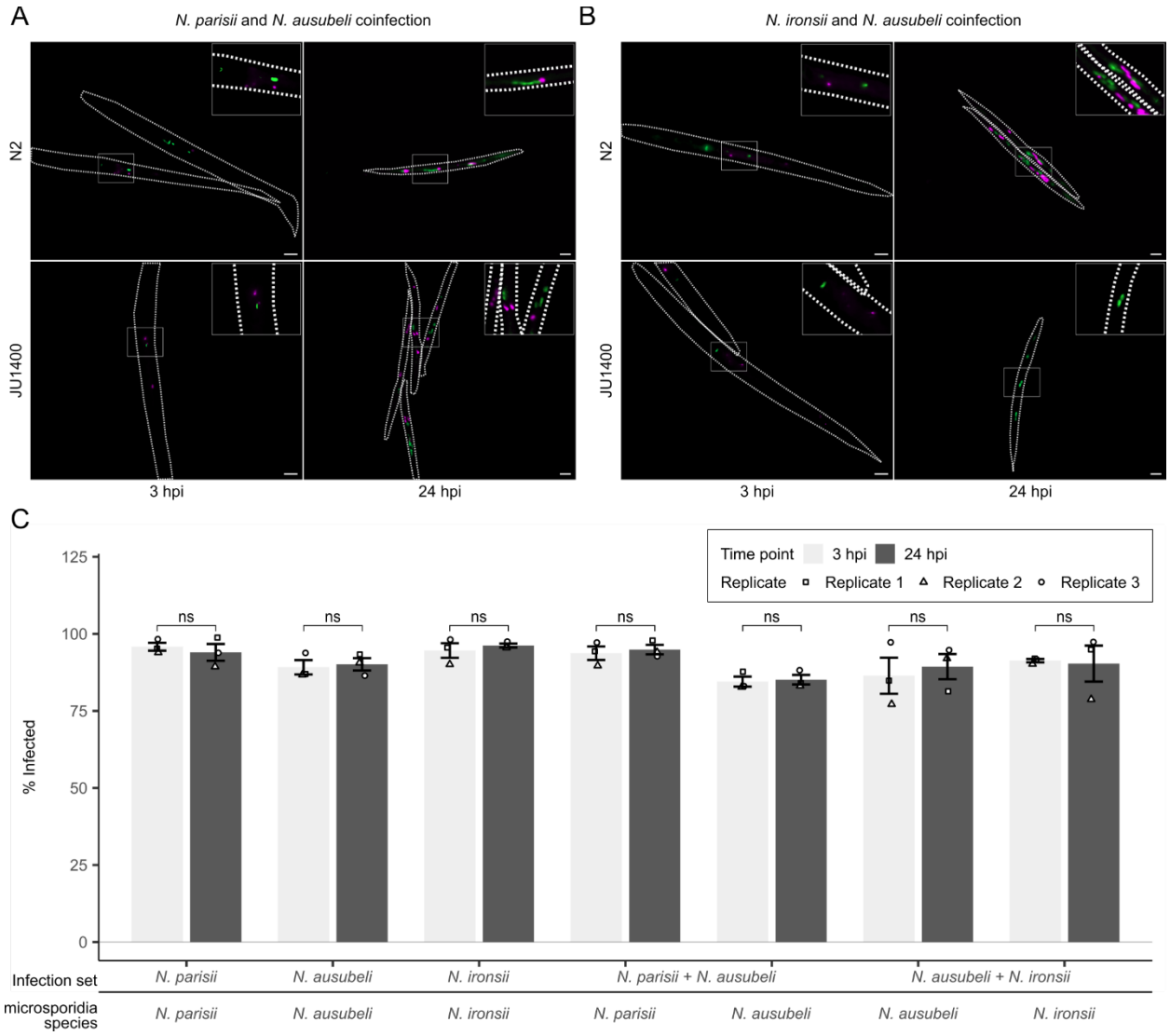

Figure S11. JU1400, but not N2, can specifically eliminate *N. ironsii* infection. N2 and JU1400 animals at the L1 stage were pulse infected for 3 hours with *N. parisii*, *N. ausubeli*, *N. ironsii, N. parisii* + *N. ausubeli, or N. ausubeli* + *N. ironsii* before washing away excess spores. Animals were either fixed immediately at 3 hpi or at 24 hpi. Samples were then stained with species-specific 18S RNA FISH probes (*N. ausubeli* = green; *N. parisii* and *N. ironsii* = magenta) and animals containing either sporoplasms or meronts were counted as infected. (A) Representative images of N2 and JU1400 infected with *N. parisii* and *N. ausubeli* (A) and *N. ironsii* and *N. ausubeli* (B). Scale bar 10 µm for 3 hpi and 25 µm for 24 hpi. Insets at top right for each

1055 image show an enlarged image of the outlined boxes. (C) Bar plot with SEM bars show percent
1056 of N2 animals infected per replicate from three biological replicates with n={59, 179} worms per
1057 replicate. p-values were determined by two-way ANOVA with Tukey post-hoc. Non-significance
1058 was defined as p > 0.05 (ns).

1059

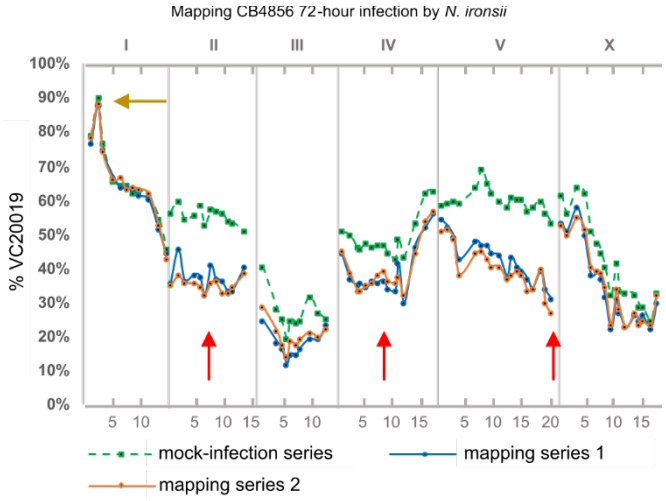

1060

1061 **Figure S12. Genetic mapping of CB4856 resistance to *N. ironsii*.** Genetic mapping of CB4856
1062 resistance to *N. ironsii* was performed with MIP-MAP using the AWR133 mapping strain. Green
1063 square-points and dotted lines represent a mock-infection replicate with the solid blue and orange
1064 lines representing two biological replicates exposed to high dose infection conditions for 72-hours
1065 per selection cycle. A red arrow on chromosome V indicates a strong signal on the right arm.
1066 Additional red arrows on chromosomes II and IV indicate broad regions of interest across the
1067 chromosomes that may contribute to CB4856 resistance phenotypes. Golden arrow indicates the
1068 *zeel-1/peel-1* incompatibility locus at chromosome I.

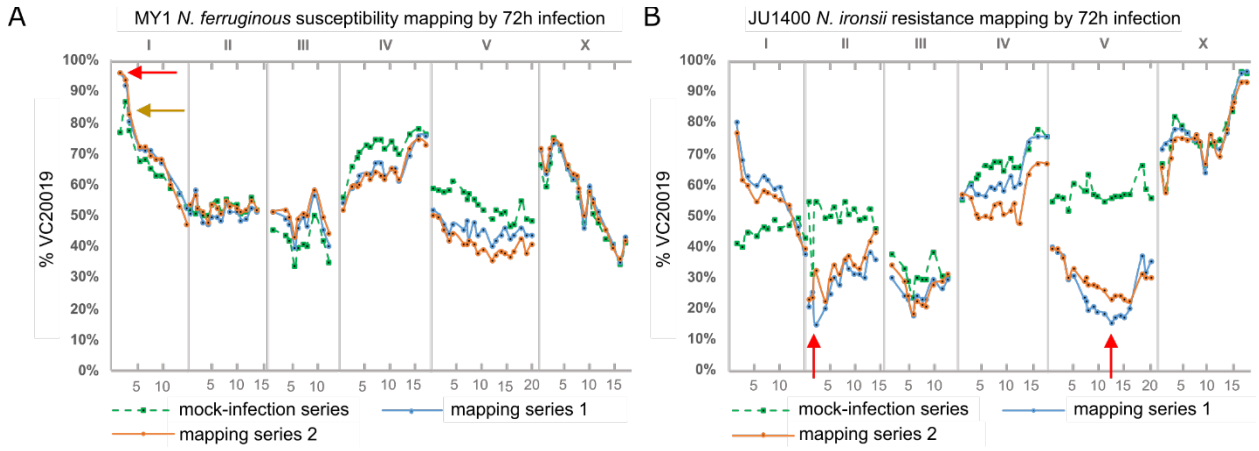

Figure S13. Genetic mapping of interaction phenotypes of JU1400 to *N. ironsii* and MY1 to *N. ferruginous* using 72-hour selections. Genetic mapping of (A) MY1 susceptibility to *N. ferruginous* and (B) JU1400 resistance to *N. ironsii* was performed with MIP-MAP using the AWR133 mapping strain. Green square-points and dotted lines represent a mock-infection replicate with the solid blue and orange lines representing two biological replicates exposed to specific infection conditions. Red arrows indicate candidate regions of interest based on the expected genome fixation direction during phenotype selection. Golden arrow indicates the *zeel-1/peel-1* incompatibility locus at chromosome I.

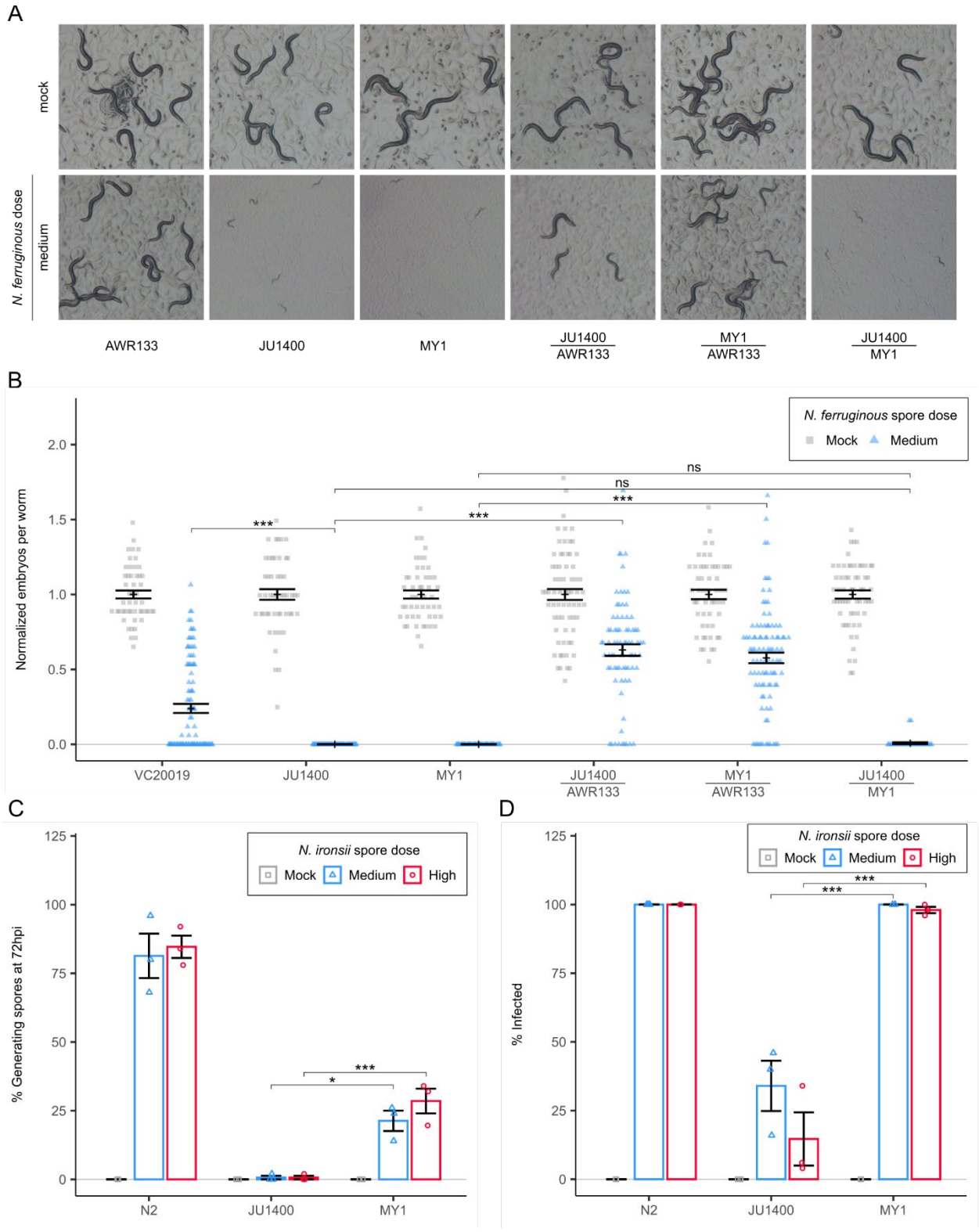

1083

1084 **Figure S14. JU1400 and MY1 susceptibility to *N. ferruginous* is recessive and MY1 is less**

1085 **resistant than JU1400 to *N. ironsii*.** (A-B) Analysis of F1 progeny from crosses between

1086 AWR133 (VC20019 with integrated pmyo-2::GFP) and the wild isolates JU1400 or MY1 as well
1087 as F1 progeny from crosses between JU1400 hermaphrodites and MY1 males. F1s were
1088 examined 72 hours post-infection by *N. ferruginous* for body size (A) and normalized embryo
1089 counts (B). (B) Dot plot with mean and SEM bars of normalized embryo counts from infected
1090 populations with a minimum of n={47,51} worms per sample. (C-D) L1 stage animals were
1091 infected for 72 hours with *N. ironsii*, fixed, and stained with DY96 and an 18S rRNA FISH probe.
1092 Bar plots depict the percent of animals with newly generated spores (C) or meront signal (D). p-
1093 values were determined by two-way ANOVA with Tukey post-hoc. Significance was defined as p
1094 ≤ 0.001 (***), p ≤ 0.05 (*) and not significant as p > 0.05 (ns).

1095

1096

1097

1098

1099

1100

1101

1102

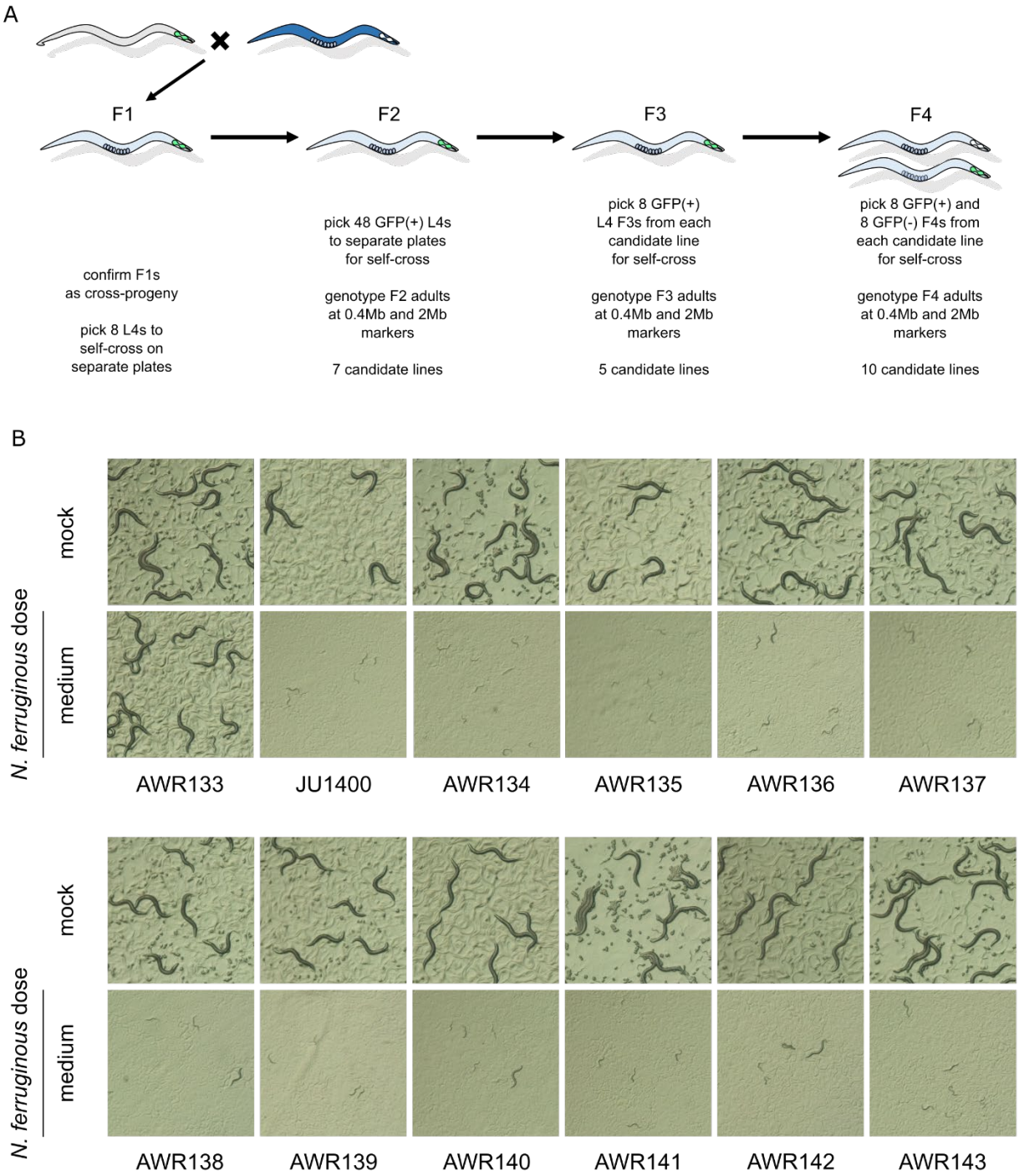

Figure S15. Generation of NILs carrying the chromosome I region that is responsible for susceptibility to *N. ferruginous*. A schematic (A) of 10 separate NILs generated through a cross between AWR133 and JU1400. These lines were infected with a medium dose of *N. ferruginous*

1107 for 72 hours (B) and their resulting body size phenotype was assessed in comparison to N2 and

1108 JU1400 control strains.

1109

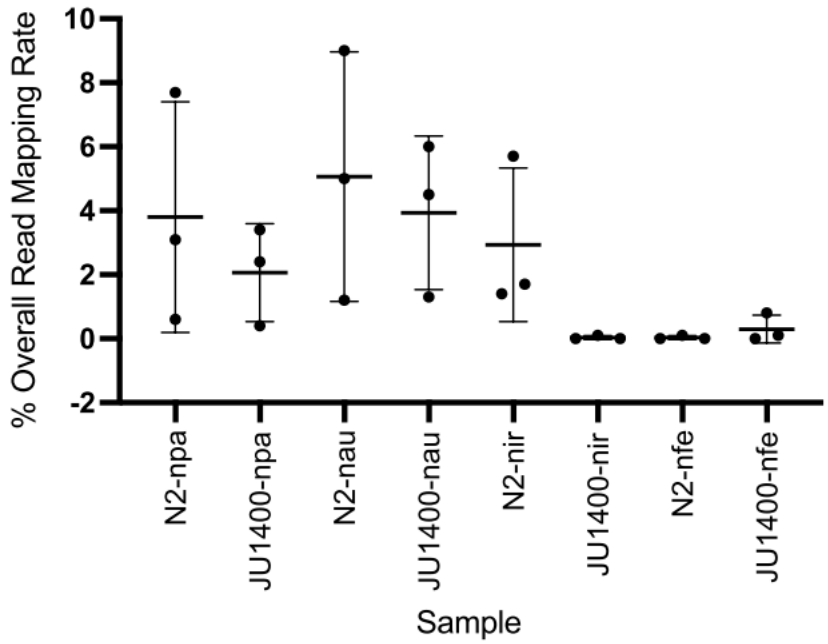

1110

1111 **Figure S16. Microsporidia mRNA reads per sample demonstrates JU1400 resistance to *N.***

1112 ***ironsii*.** Scatterplot of overall read mapping rate of *Nematocida* in both strains with mean and

1113 standard deviation. uni (uninfected), npa (*N. parisii)*, nau (*N. ausubeli*), nir (*N. ironsii),* and nfe (*N.*

1114 *ferruginous)*.

A

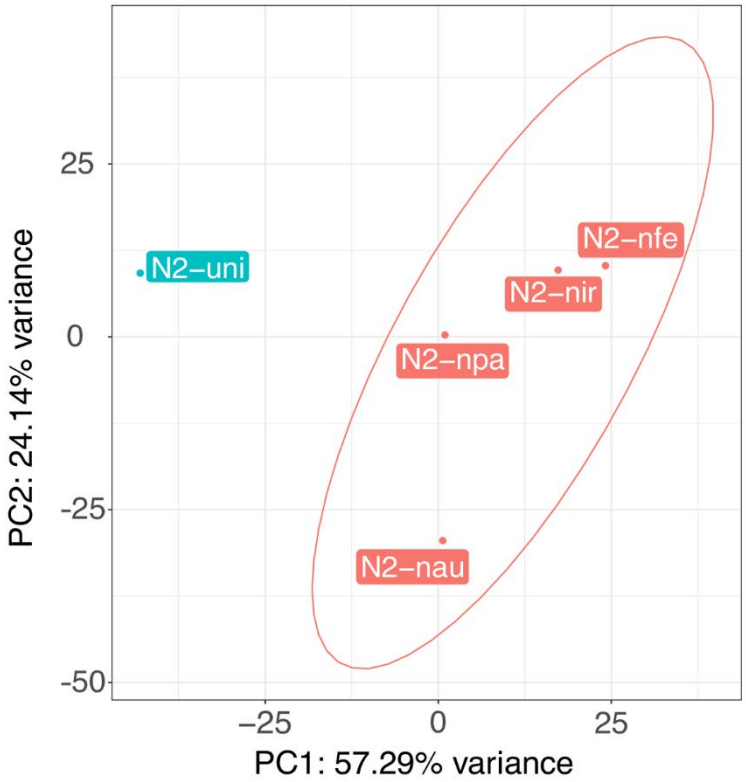

B

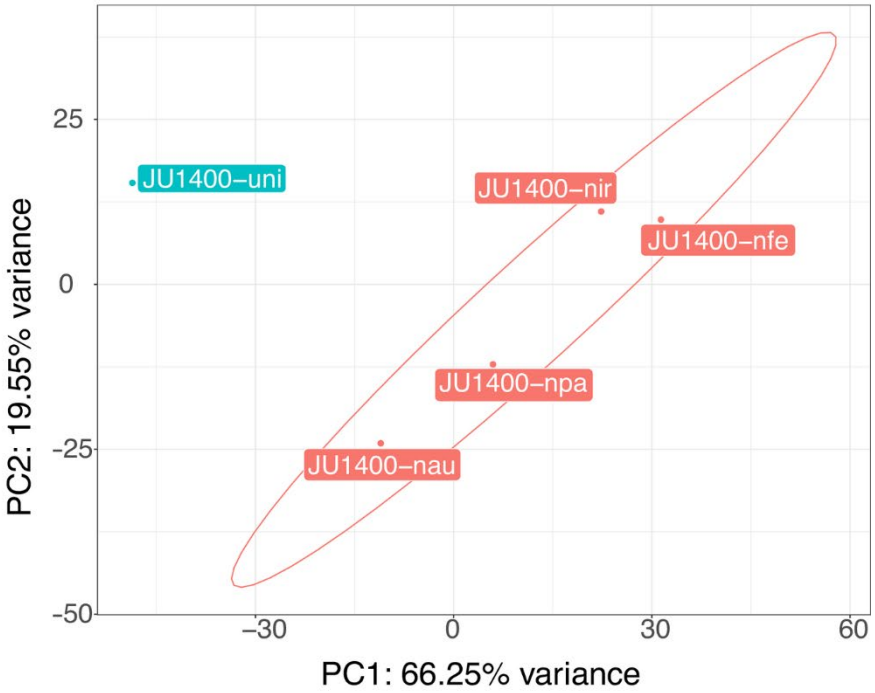

1115 Infection: Infected Uninfected

1116 **Figure S17. Principal component analysis of N2 and JU1400 samples.** Principal component
1117 plots of expression data from only (A) N2 samples or (B) JU1400 samples. Circles represent
1118 confidence ellipses around each strain at 95% confidence interval. uni (uninfected), npa (*N.*
1119 *parisii)*, nau (*N. ausubeli*), nir (*N. ironsii),* and nfe (*N. ferruginous)*.

1120

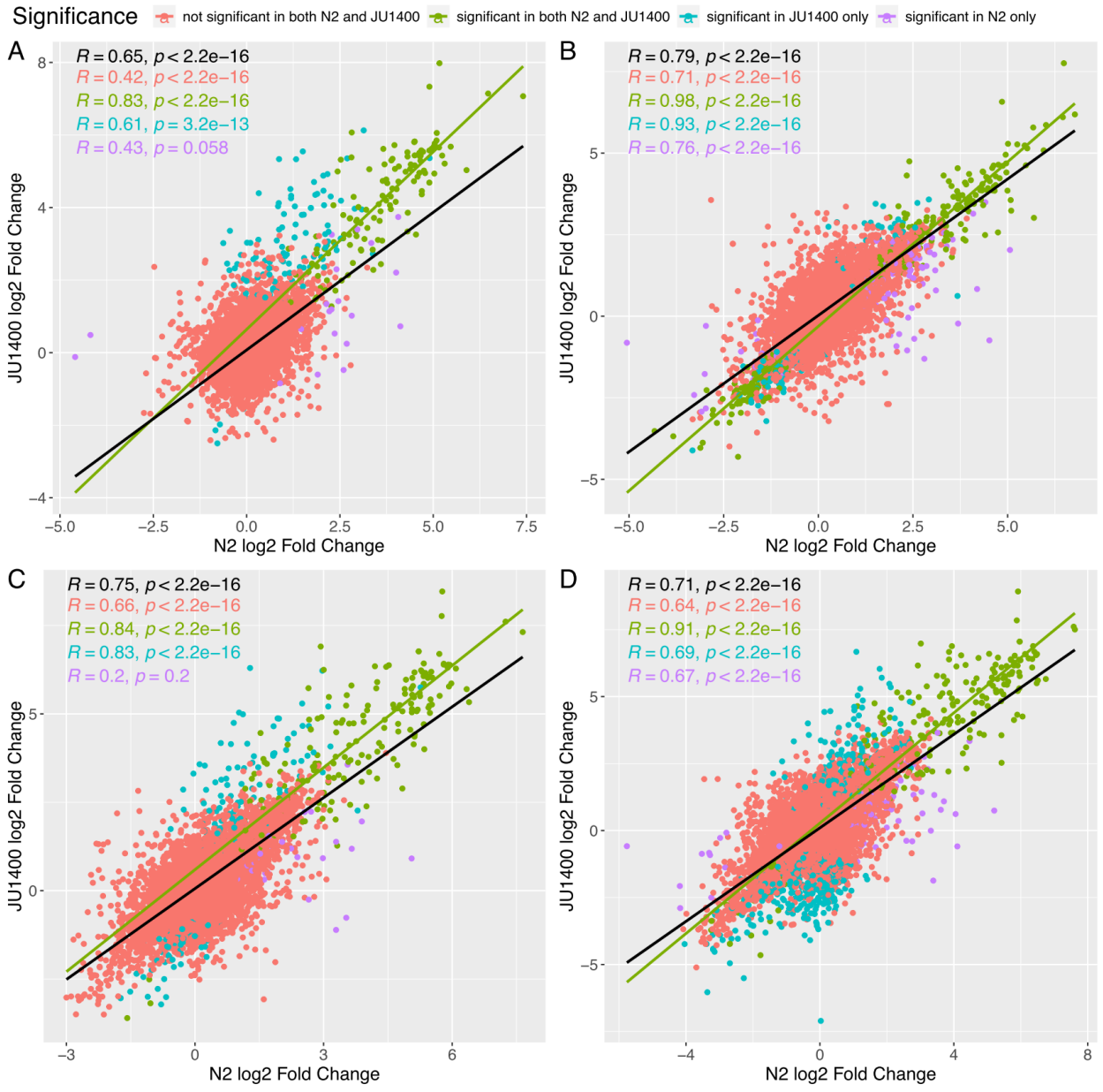

1121

1122 **Figure S18. Comparison of correlation between N2 and JU1400 strains after infection with**
1123 **different microsporidia species.** Correlation between log_2 fold changes in genes of N2 and
1124 JU1400 animals infected with (A) *N. parisii* (B) *N. ausubeli* (C) *N. ironsii* (D) *N. ferruginous*.
1125 Pearson's correlation value and p-value for each cluster (pink, green, blue, purple) are presented
1126 in the upper left corner. Pearson's correlation value and p-value for all the genes are presented
1127 in the bottom left corner. A gene with FDR adjusted p-value of <0.01 is deemed significant in each
1128 strain.

1129

1130

1131

1132

1133

1134

1135

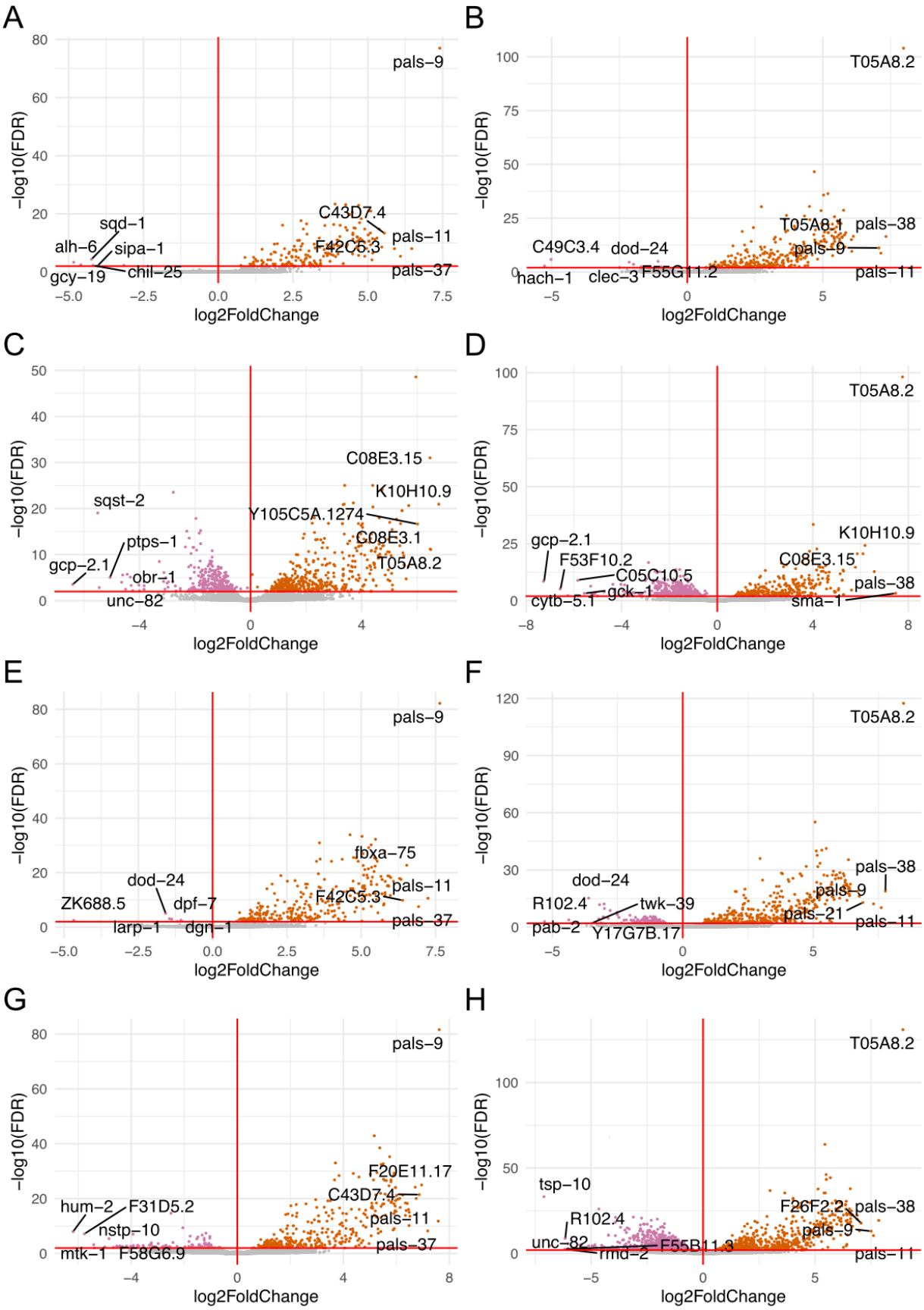
A
pals−9
sqd−1
alh−6
sipa−1
gcy−19
chil−25
C43D7.4
F42C5.3
pals−11
pals−37
−log10(FDR)
log2FoldChange
B
T05A8.2
T05A8.1
pals−38
pals−9
C49C3.4
dod−24
hach−1
clec−3
F55G11.2
pals−11
C
C08E3.15
K10H10.9
sqst−2
Y105C5A.1274
C08E3.1
ptps−1
T05A8.2
gcp−2.1
obr−1
unc−82
D
T05A8.2
K10H10.9
gcp−2.1
F53F10.2
C05C10.5
C08E3.15
pals−38
gck−1
cytb−5.1
sma−1
E
pals−9
fbxa−75
dod−24
pals−11
ZK688.5
dpf−7
F42C5.3
larp−1
dgn−1
pals−37
F
T05A8.2
pals−38
dod−24
pals−9
R102.4
twk−39
pals−21
pab−2
Y17G7B.17
pals−11
G
pals−9
F20E11.17
C43D7.4
hum−2
F31D5.2
pals−11
nstp−10
pals−37
mtk−1
F58G6.9
H
T05A8.2
tsp−10
F26F2.2
pals−38
R102.4
pals−9
unc−82
rmd−2
F55B11.3
pals−11

1136

1137

1138 **Figure S19. Volcano plots of differentially regulated genes.** (A) *N. parisii*-infected N2. (B) *N.*
1139 *parisii*-infected JU1400. (C) *N. ausubeli*-infected N2. (D) *N. ausubeli*-infected JU1400. (E) *N.*
1140 *ironsii*-infected N2. (F) *N. ironsii*-infected JU1400. (G) *N. ferruginous*-infected N2. (H) *N.*
1141 *ferruginous*-infected JU1400. Each point represents a gene, orange points indicate differentially
1142 upregulated genes, pink points are differentially downregulated genes while grey points represent
1143 genes with FDR-adjusted p-value >0.01 (red horizontal line). The top five differentially
1144 upregulated and downregulated genes with FDR-adjusted p-value <0.01 are labelled with their
1145 respective gene names.

1146

1147

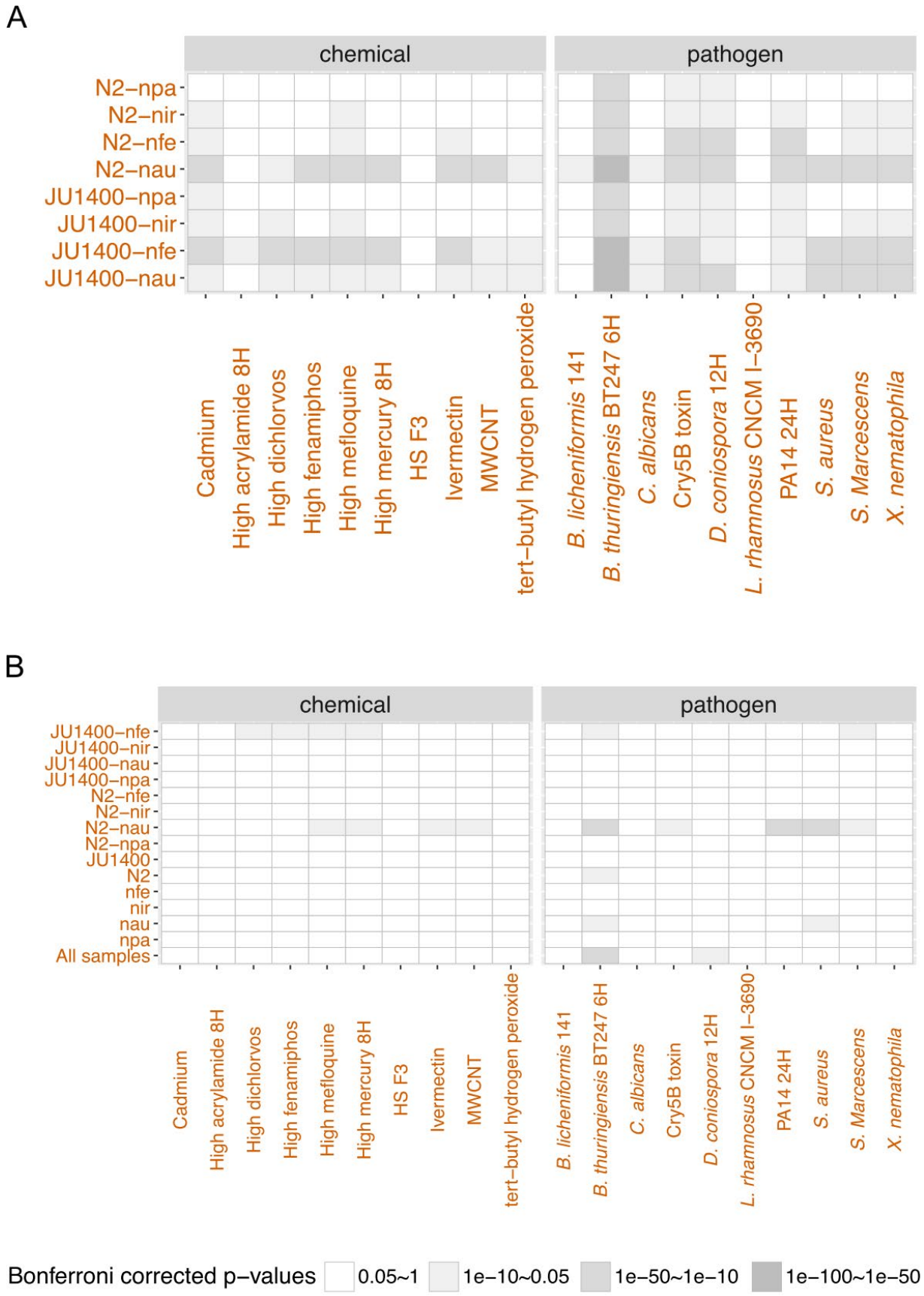
A
chemical
pathogen
N2−npa
N2−nir
N2−nfe
N2−nau
JU1400−npa
JU1400−nir
JU1400−nfe
JU1400−nau
Cadmium
High acrylamide 8H
High dichlorvos
High fenamiphos
High mefloquine
High mercury 8H
HS F3
Ivermectin
MWCNT
tert−butyl hydrogen peroxide
B. licheniformis 141
B. thuringiensis BT247 6H
C. albicans
Cry5B toxin
D. coniospora 12H
L. rhamnosus CNCM I−3690
PA14 24H
S. aureus
S. Marcescens
X. nematophila
B
chemical
pathogen
JU1400−nfe
JU1400−nir
JU1400−nau
JU1400−npa
N2−nfe
N2−nir
N2−nau
N2−npa
JU1400
N2
nfe
nir
nau
npa
All samples
Cadmium
High acrylamide 8H
High dichlorvos
High fenamiphos
High mefloquine
High mercury 8H
HS F3
Ivermectin
MWCNT
tert−butyl hydrogen peroxide
B. licheniformis 141
B. thuringiensis BT247 6H
C. albicans
Cry5B toxin
D. coniospora 12H
L. rhamnosus CNCM I−3690
PA14 24H
S. aureus
S. Marcescens
X. nematophila
Bonferroni corrected p−values
0.05~1
1e−10~0.05
1e−50~1e−10
1e−100~1e−50

1148

1149 **Figure S20. Overlap between the significant upregulated genes upon microsporidia**
1150 **infection and differentially expressed datasets of *C. elegans* genes upon exposure to**
1151 **chemicals or bacterial infection.** (A) upregulated genes from microsporidia-infected samples.
1152 (B) upregulated gens from strain specific, pathogen specific, and strain-pathogen specific gene
1153 sets. uni (uninfected), npa (*N. parisii)*, nau (*N. ausubeli*), nir (*N. ironsii),* and nfe (*N. ferruginous)*.

1154

1155

1156

1157

1158

1159 **Table 1. PhenoMIP screen interaction hits**

Strain	Site of isolation	Microsporidia species	Relative Impact on host fitness	Modified z-score	Single infection embryo phenotype?
AB1	Adelaide, Australia	*N. ferruginous*	Increase	1.65, 1.64	Yes
JU397	Ouistreham, France	*N. ferruginous*	Increase	2.58, 2.59	Yes
LKC34	Antananarivo, Madagascar	*N. ferruginous*	Increase	2.14, 2.40	Untested
ED3040	Johannesburg, South Africa	*N. ferruginous*	Decrease	-1.90, -1.90	Untested
ED3042	Capetown, South Africa	*N. ferruginous*	Decrease	-2.53, -1.57	Yes
JU360	Franconville, France	*N. ferruginous*	Decrease	-2.68, -2.74	Yes
MY1	Munster, Germany	*N. ferruginous*	Decrease	-6.05, -6.05 -4.52[M], -4.25[M] -2.17[L] -1.85[L]	Yes
JU1400	Sevilla, Spain	*N. ferruginous*	Decrease	-6.43, -6.43 -3.33[M], -3.33[M]	Yes
CB4856	Hawaii, USA	*N. ironsii*	Increase	2.48, 2.88	Yes
JU300	Le Blanc, France	*N. ironsii*	Increase	2.19, 2.70	No
MY2	Munster, Germany	*N. ironsii*	Decrease	-2.83, -3.50	Yes
JU533	Primel-Tregastel, France	*N. ironsii*	Decrease	-2.00, -2.00	Untested
JU642	Paris, France	*N. ironsii*	Decrease	-2.44, -3.06	Untested
JU1400	Sevilla, Spain	*N. ironsii*	Decrease	-1.78, -1.78	Yes
JU360	Franconville, France	*N. ausubeli*	Increase	2.03, 1.88	No
MY2	Munster, Germany	*N. ausubeli*	Decrease	-2.07, -2.42	No

1160 All modified z-scores are identified from high dose infections unless otherwise noted.

1161 [M] Medium dose infection modified z-score

1162 [L] Low dose infection modified z-score

1163

1164

1165 **Table S1. Microsporidia species information.**

Microsporidia species	Original host	Infected tissue	Geographical origin
Nematocida parisii [15]	*C. elegans*	Intestine	France
Nematocida ausubeli [15,32]	*C. briggsae*	Intestine	India
Nematocida ironsii [19,43]	*C. briggsae*	Intestine	Hawaii
Nematocida ferruginous [44]	*C. elegans*	Epidermis/muscle	France

1166

1167 **Table S2. PhenoMIP microsporidia infection doses.**

Microsporidia species	Microsporidia strain	Infection round	Spores per cm^2 media		
			Low	**Medium**	**High**
Nematocida parisii	ERTm1	1	8,000	16,000	32,000
		2-4	13,269	26,539	53,078
		Follow-up infections		26,539	53,078
Nematocida ausubeli	ERTm2	1	26,539	NA	53,078
		2-4	26,539	39,808	53,078
		Follow-up infections		17,692	53,078
Nematocida ironsii	ERTm5	1	22,116	44,232	88,464
		2-4	30,692	61,924	123,849
		Follow-up infections		61,924	123,849
Nematocida ferruginous	LUAm1	1	88,464	176,928	353,857
		2-3	159,235	318,471	636,942
		4	159,235	318,471	751,592
		Follow-up infections		318,471	751,592
	LUAm3	**Follow-up infections**		353,857	
Nematocida cider	AWRm77	**Follow-up infections**		141,542	

1168 * effective dose of spores used in retests and additional infections

1169

1170 **Table S3. Wild isolate mapping microsporidia infection doses.**

Wild isolate strain(s)	Microsporidia strain	Infection time (hours)	Infection round	Spores per cm^2 media
JU1400, MY1	*Nematocida ferruginous*	72	1-2	350,318
			3	445,859
JU1400	*Nematocida ironsii*	72	1	178,343
			2-3	254,777
JU1400	*Nematocida ironsii*	96	1-2	509,554

CB4856	*Nematocida ironsii*	72	1	178,343
			2-3	254,777

1171

1172 **Table S4. NIL strain chromosome I region composition.**

Strain	I:491,763	I:1,051,810	I:1,567,450	I:2,012,869	GFP Status I-2,851,135
AWR134	JU1400	JU1400	JU1400	--	+
AWR135	JU1400	JU1400	JU1400	JU1400	-
AWR136	JU1400	JU1400	JU1400	JU1400	+
AWR137	JU1400	JU1400	JU1400	JU1400	-
AWR138	JU1400	--	--	--	+
AWR139	JU1400	JU1400	JU1400	JU1400	-
AWR140	JU1400	JU1400	--	--	+
AWR141	JU1400	JU1400	JU1400	JU1400	-
AWR142	JU1400	JU1400	--	--	+
AWR143	JU1400	JU1400	JU1400	JU1400	-

1173

1174 **Table S9. Gene classes and domains used for enrichment analyses.**

1175

Domain/ Gene Family	Databse	Wormbase gene class OR Pfam ID
F-box	Wormbase	fbxa, fbxb, fbxc
MATH (meprin or Traf homology) or BATH (BTB and MATH domain-containing)	Wormbase	math, bath
PALS (protein containing ALS2CR12 signature)	Wormbase	pals
C-type lectins	Wormbase	clec
DUF713	Pfam	PF015218
DUF684	Pfam	PF05075
chil	Wormbase	chil
Histone	Pfam	PF00125
Nematode cuticle collagen N-terminal domain	Pfam	PF01484
skr (Skp1-related)	Wormbase	Skr
Other (Any genes not in the domain or gene family above)	-	-

1176

1177

1178 **Table S11. Published data sets from WormExp used in this study.**

Chemical/Pathogen	WormExp Term
Cadmium	• down by Cadmium (Huffman)

	• UP by Cadmium (Huffman)
Dichlorvos	• Down by high dichlorvos • UP by high dichlorvos
Fenamiphos	• Down by fenamiphos high • UP by fenamiphos high
Mercury	• Down by mercury high 8H • UP by mercury high 8H
Ivermectin (IVM)	• Down by 1ng/ml ivermectin • UP by 1ng/ml ivermectin
Mefloquine	• Down by mefloquine high • UP by mefloquine high
Heat Shock F3	• Down HS F3 vs. CTL F3 • UP HS F3 vs. CTL F3
Acrylamide	• Down by high acrylamide 8H • UP by high acrylamide 8H
Multi-walled carbon nanotubes (MWCNT)	• Down by MWCNT 24H vs. 0H • UP by MWCNT 24H vs. 0H
Tert-butyl hydrogen peroxide	• down by tert-butyl hydrogen peroxide (Oliveira) • UP by tert-butyl hydrogen peroxide (Oliveira)
Bacillus thuringiensis strain BT247	• down by B. thuringiensis at 6h (BT247, 1:2) (Yang) • down by B. thuringiensis at 6h (BT247, 1:2) (Yang)
Bacillus licheniformis strain 141	• down by B. licheniformis 141 • UP by B. licheniformis 141
Drechmeria coniospora	• Down D. coniospora 12h, RNASeq • UP D. coniospora 12h, RNASeq
Pseudomonas aeruginosa strain PA14	• down by PA14, 24h • UP by PA14, 24h
Cry5B toxin	• down by Bt toxin,Cry5B • UP by Bt toxin,Cry5B
Candida albicans	• down by C. albicans (Pukkila-Worley) • UP by C. albicans (Pukkila-Worley)
Lactobacillus rhamnosus strain CNCM I-3690	• Down fed with L. rhamnosus CNCM I-3690 vs. OP50,3 days • UP fed with L. rhamnosus CNCM I-3690 vs. OP50,3 days
Staphylococcus aureus	• down by S. aureus (Bond) • UP by S. aureus (Bond)
Serratia marcescens	• Down infected by S. Marcescens • UP on S. marcescens
Xenorhabdus nematophila	• Down infected by X. Nematophila

	• UP on X. nematophila

1179

1180 **References**

1181 1. Band G, Rockett KA, Spencer CCA, Kwiatkowski DP. A novel locus of resistance to
1182 severe malaria in a region of ancient balancing selection. Nature. 2015;526: 253–257.
1183 doi:10.1038/nature15390

1184 2. Samson M, Libert F, Doranz BJ, Rucker J, Liesnard C, Farber CM, et al. Resistance to
1185 HIV-1 infection in caucasian individuals bearing mutant alleles of the CCR-5 chemokine
1186 receptor gene. Nature. 1996;382: 722–725. doi:10.1038/382722a0

1187 3. Sabeti PC, Schaffner SF, Fry B, Lohmueller J, Varilly P, Shamovsky O, et al. Positive
1188 natural selection in the human lineage. Science. 2006;312: 1614–1620.
1189 doi:10.1126/science.1124309

1190 4. Lazzaro BP, Sceurman BK, Clark AG. Genetic Basis of Natural Variation in D.
1191 melanogaster Antibacterial Immunity. Science. 2004;303: 1873–1876.
1192 doi:10.1126/science.1092447

1193 5. Duxbury EM, Day JP, Maria Vespasiani D, Thüringer Y, Tolosana I, Smith SC, et al. Host-
1194 pathogen coevolution increases genetic variation in susceptibility to infection. eLife.
1195 2019;8: 1–21. doi:10.7554/eLife.46440

1196 6. Lazzaro BP, Sackton TB, Clark AG. Genetic variation in Drosophila melanogaster
1197 resistance to infection: A comparison across bacteria. Genetics. 2006;174: 1539–1554.
1198 doi:10.1534/genetics.105.054593

1199 7. Schulenburg H, Ewbank JJ. Diversity and specificity in the interaction between
1200 Caenorhabditis elegans and the pathogen Serratia marcescens. BMC Evolutionary Biology.
1201 2004;4: 49. doi:10.1186/1471-2148-4-49

1202 8. Marquet S. Overview of human genetic susceptibility to malaria: From parasitemia control
1203 to severe disease. Infect Genet Evol. 2018;66: 399–409. doi:10.1016/j.meegid.2017.06.001

1204 9. Raberg L, Sim D, Read AF. Disentangling genetic variation for resistance and tolerance to
1205 infectious diseases in animals. Science. 2007;318: 812–814. doi:10.1126/science.1148526

1206 10. Medzhitov R, Schneider DS, Soares MP. Disease tolerance as a defense strategy. Science.
1207 2012;335: 936–941. doi:10.1126/science.1214935

1208 11. Wadi L, Reinke AW. Evolution of microsporidia: An extremely successful group of
1209 eukaryotic intracellular parasites. PLoS Pathog. 2020;16: e1008276.
1210 doi:10.1371/journal.ppat.1008276

1211 12. Stentiford GD, Feist SW, Stone DM, Bateman KS, Dunn AM. Microsporidia: diverse,
1212 dynamic, and emergent pathogens in aquatic systems. Trends Parasitol. 2013;29: 567–578.
1213 doi:10.1016/j.pt.2013.08.005

1214 13. Murareanu BM, Sukhdeo R, Qu R, Jiang J, Reinke AW, Weiss LM. Generation of a
1215 Microsporidia Species Attribute Database and Analysis of the Extensive Ecological and
1216 Phenotypic Diversity of Microsporidia. mBio. 2021. pp. e01490-21.

1217 14. Willis AR, Reinke AW. Factors That Determine Microsporidia Infection and Host
1218 Specificity. Exp Suppl. 2022;114: 91–114. doi:10.1007/978-3-030-93306-7_4

1219 15. Troemel ER, Felix M-A, Whiteman NK, Barriere A, Ausubel FM. Microsporidia are
1220 natural intracellular parasites of the nematode Caenorhabditis elegans. PLoS Biol. 2008;6:
1221 2736–2752. doi:10.1371/journal.pbio.0060309

1222 16. Balla KM, Luallen RJ, Bakowski MA, Troemel ER. Cell-to-cell spread of microsporidia
1223 causes Caenorhabditis elegans organs to form syncytia. Nature Microbiology. 2016;1:
1224 16144.

1225 17. Higes M, Martín-Hernández R, Botías C, Bailón EG, González-Porto AV, Barrios L, et al.
1226 How natural infection by Nosema ceranae causes honeybee colony collapse. Environ
1227 Microbiol. 2008;10: 2659–2669. doi:10.1111/j.1462-2920.2008.01687.x

1228 18. Richaud A, Zhang G, Lee D, Lee J, Félix M-A. The Local Coexistence Pattern of Selfing
1229 Genotypes in Caenorhabditis elegans Natural Metapopulations. Genetics. 2018;208: 807–
1230 821. doi:10.1534/genetics.117.300564

1231 19. Balla KM, Andersen EC, Kruglyak L, Troemel ER. A Wild C. Elegans Strain Has
1232 Enhanced Epithelial Immunity to a Natural Microsporidian Parasite. PLoS Pathogens.
1233 2015;11: e1004583. doi:10.1371/journal.ppat.1004583

1234 20. Tamim El Jarkass H, Mok C, Schertzberg MR, Fraser AG, Troemel ER, Reinke AW. An
1235 intestinally secreted host factor promotes microsporidia invasion of C. elegans. Lourido S,
1236 Sengupta P, editors. eLife. 2022;11: e72458. doi:10.7554/eLife.72458

1237 21. Capaul M, Ebert D. Parasite-Mediated Selection in Experimental Daphnia Magna
1238 Populations. Evolution. 2003;57: 249–260. doi:10.1111/j.0014-3820.2003.tb00260.x

1239 22. Haag CR, Ebert D. Parasite–mediated selection in experimental metapopulations of
1240 Daphnia magna. Proceedings of the Royal Society of London Series B: Biological Sciences.
1241 2004;271: 2149–2155. doi:10.1098/rspb.2004.2841

1242 23. Huang Q, Lattorff HMG, Kryger P, Conte YL, Moritz RFA. A selective sweep in a
1243 microsporidian parasite Nosema-tolerant honeybee population, Apis mellifera. Animal
1244 Genetics. 2014;45: 267–273. doi:10.1111/age.12114

1245 24. Keller D, Kirk D, Luijckx P. Four QTL underlie resistance to a microsporidian parasite that
1246 may drive genome evolution in its Daphnia host. bioRxiv. 2019; 847194.
1247 doi:10.1101/847194

1248 25. Krebs M, Routtu J, Ebert D. QTL mapping of a natural genetic polymorphism for long-term
1249 parasite persistence in Daphnia populations. Parasitology. 2017;144: 1686–1694.
1250 doi:10.1017/S0031182017001032

1251 26. Routtu J, Ebert D. Genetic architecture of resistance in Daphnia hosts against two species of
1252 host-specific parasites. Heredity (Edinb). 2015;114: 241–248. doi:10.1038/hdy.2014.97

1253 27. King KC, Brockhurst MA, Vasieva O, Paterson S, Betts A, Ford SA, et al. Rapid evolution
1254 of microbe-mediated protection against pathogens in a worm host. The ISME Journal.
1255 2016;10: 1915–1924. doi:10.1038/ismej.2015.259

1256 28. Morran LT, Schmidt OG, Gelarden IA, Parrish RC, Lively CM. Running with the Red
1257 Queen: Host-Parasite Coevolution Selects for Biparental Sex. Science. 2011;333: 216–218.
1258 doi:10.1126/science.1206360

1259 29. Papkou A, Guzella T, Yang W, Koepper S, Pees B, Schalkowski R, et al. The genomic
1260 basis of Red Queen dynamics during rapid reciprocal host–pathogen coevolution. PNAS.
1261 2019;116: 923–928. doi:10.1073/pnas.1810402116

1262 30. Masri L, Branca A, Sheppard AE, Papkou A, Laehnemann D, Guenther PS, et al. Host–
1263 Pathogen Coevolution: The Selective Advantage of Bacillus thuringiensis Virulence and Its
1264 Cry Toxin Genes. PLOS Biology. 2015;13: e1002169. doi:10.1371/journal.pbio.1002169

1265 31. Schulenburg H, Félix M-A. The Natural Biotic Environment of . Genetics. 2017;206: 55–
1266 86.

1267 32. Zhang G, Sachse M, Prevost M-C, Luallen RJ, Troemel ER, Felix M-A. A Large Collection
1268 of Novel Nematode-Infecting Microsporidia and Their Diverse Interactions with
1269 Caenorhabditis elegans and Other Related Nematodes. PLoS Pathog. 2016;12: e1006093.
1270 doi:10.1371/journal.ppat.1006093

1271 33. Cook DE, Zdraljevic S, Roberts JP, Andersen EC. CeNDR, the Caenorhabditis elegans
1272 natural diversity resource. Nucleic Acids Research. 2017. doi:10.1093/nar/gkw893

1273 34. Ashe A, Bélicard T, Le Pen J, Sarkies P, Frézal L, Lehrbach NJ, et al. A deletion
1274 polymorphism in the Caenorhabditis elegans RIG-I homolog disables viral RNA dicing and
1275 antiviral immunity. eLife. 2013;2013: 1–21. doi:10.7554/eLife.00994.001

1276 35. Sterken MG, van Sluijs L, Wang YA, Ritmahan W, Gultom ML, Riksen JAG, et al.
1277 Punctuated Loci on Chromosome IV Determine Natural Variation in Orsay Virus
1278 Susceptibility of Caenorhabditis elegans Strains Bristol N2 and Hawaiian CB4856. Journal
1279 of Virology. 2021;95: e02430-20. doi:10.1128/JVI.02430-20

1280 36. Reddy KC, Andersen EC, Kruglyak L, Kim DH. A Polymorphism in npr-1 Is a Behavioral
1281 Determinant of Pathogen Susceptibility in C. elegans. Science. 2009;323: 382–384.
1282 doi:10.1126/science.1166527

1283 37. Huang Y, Kammenga JE. Genetic Variation in Caenorhabditis elegans Responses to
1284 Pathogenic Microbiota. Microorganisms. 2020;8: 618.
1285 doi:10.3390/microorganisms8040618

1286 38. Webster AK, Hung A, Moore BT, Guzman R, Jordan JM, Kaplan REW, et al. Population
1287 Selection and Sequencing of Caenorhabditis elegans Wild Isolates Identifies a Region on
1288 Chromosome III Affecting Starvation Resistance. G3: Genes, Genomes, Genetics. 2019;9:
1289 3477–3488. doi:10.1534/g3.119.400617

1290 39. Mok C, Belmarez G, Edgley ML, Moerman DG, Waterston RH. PhenoMIP: High-
1291 Throughput Phenotyping of Diverse Caenorhabditis elegans Populations via Molecular
1292 Inversion Probes. G3: Genes, Genomes, Genetics. 2020;10: 3977–3990.
1293 doi:10.1534/g3.120.401656

1294 40. Webster AK, Chitrakar R, Powell M, Chen J, Fisher K, Tanny RE, et al. Using population
1295 selection and sequencing to characterize natural variation of starvation resistance in
1296 Caenorhabditis elegans. Hobert O, James DE, McGrath P, editors. eLife. 2022;11: e80204.
1297 doi:10.7554/eLife.80204

1298 41. Luallen RJ, Reinke AW, Tong L, Botts MR, Felix M-A, Troemel ER. Discovery of a
1299 Natural Microsporidian Pathogen with a Broad Tissue Tropism in Caenorhabditis elegans.
1300 PLoS Pathog. 2016;12: e1005724. doi:10.1371/journal.ppat.1005724

1301 42. Murareanu BM, Antao NV, Zhao W, Dubuffet A, El Alaoui H, Knox J, et al. High-
1302 throughput small molecule screen identifies inhibitors of microsporidia invasion and
1303 proliferation in C. elegans. Nat Commun. 2022;13: 5653. doi:10.1038/s41467-022-33400-y

1304 43. Reinke AW, Balla KM, Bennett EJ, Troemel ER. Identification of microsporidia host-
1305 exposed proteins reveals a repertoire of rapidly evolving proteins. Nat Commun. 2017;8:
1306 14023. doi:10.1038/ncomms14023

1307 44. Wadi L, El Jarkass HT, Tran TD, Islah N, Luallen RJ, Reinke AW. Genomic and
1308 phenotypic evolution of nematode-infecting microsporidia. bioRxiv. 2022;
1309 2022.08.28.505597. doi:10.1101/2022.08.28.505597

1310 45. Jarkass HTE, Reinke AW. The ins and outs of host-microsporidia interactions during
1311 invasion, proliferation and exit. Cellular Microbiology. 2020;22: e13247.
1312 doi:10.1111/cmi.13247

1313 46. Tecle E, Troemel ER. Insights from C. elegans into Microsporidia Biology and Host-
1314 Pathogen Relationships. Exp Suppl. 2022;114: 115–136. doi:10.1007/978-3-030-93306-7_5

1315 47. Reddy KC, Dror T, Sowa JN, Panek J, Chen K, Lim ES, et al. An Intracellular Pathogen
1316 Response Pathway Promotes Proteostasis in C. elegans. Curr Biol. 2017;27: 3544-3553.e5.
1317 doi:10.1016/j.cub.2017.10.009

1318 48. Reddy KC, Dror T, Underwood RS, Osman GA, Elder CR, Desjardins CA, et al.
1319 Antagonistic paralogs control a switch between growth and pathogen resistance in C.
1320 elegans. PLoS Pathog. 2019;15: e1007528. doi:10.1371/journal.ppat.1007528

1321 49. Willis AR, Zhao W, Sukhdeo R, Wadi L, Jarkass HTE, Claycomb JM, et al. A parental
1322 transcriptional response to microsporidia infection induces inherited immunity in offspring.
1323 Science Advances. 2021;7: eabf3114. doi:10.1126/sciadv.abf3114

1324 50. Tecle E, Chhan CB, Franklin L, Underwood RS, Hanna-Rose W, Troemel ER. The purine
1325 nucleoside phosphorylase pnp-1 regulates epithelial cell resistance to infection in C.
1326 elegans. PLOS Pathogens. 2021;17: e1009350. doi:10.1371/journal.ppat.1009350

1327 51. Balla KM, Lažetić V, Troemel ER. Natural variation in the roles of C. elegans autophagy
1328 components during microsporidia infection. PLOS ONE. 2019;14: e0216011.
1329 doi:10.1371/journal.pone.0216011

1330 52. Mok CA, Au V, Thompson OA, Edgley ML, Gevirtzman L, Yochem J, et al. MIP-MAP:
1331 High-Throughput Mapping of Caenorhabditis elegans Temperature-Sensitive Mutants via
1332 Molecular Inversion Probes. Genetics. 2017;207: 447–463.
1333 doi:10.1534/genetics.117.300179

1334 53. Seidel HS, Ailion M, Li J, Oudenaarden A van, Rockman MV, Kruglyak L. A Novel
1335 Sperm-Delivered Toxin Causes Late-Stage Embryo Lethality and Transmission Ratio
1336 Distortion in C. elegans. PLOS Biology. 2011;9: e1001115.
1337 doi:10.1371/journal.pbio.1001115

1338 54. Bakowski MA, Desjardins CA, Smelkinson MG, Dunbar TL, Lopez-Moyado IF, Rifkin
1339 SA, et al. Ubiquitin-mediated response to microsporidia and virus infection in C. elegans.
1340 PLoS Pathog. 2014;10: e1004200. doi:10.1371/journal.ppat.1004200

1341 55. Panek J, Gang SS, Reddy KC, Luallen RJ, Fulzele A, Bennett EJ, et al. A cullin-RING
1342 ubiquitin ligase promotes thermotolerance as part of the intracellular pathogen response in
1343 Caenorhabditis elegans. Proceedings of the National Academy of Sciences. 2020;117:
1344 7950–7960. doi:10.1073/pnas.1918417117

1345 56. Yang W, Dierking K, Schulenburg H. WormExp: a web-based application for a
1346 Caenorhabditis elegans-specific gene expression enrichment analysis. Bioinformatics.
1347 2016;32: 943–945. doi:10.1093/bioinformatics/btv667

1348 57. Lewis JA, Szilagyi M, Gehman E, Dennis WE, Jackson DA. Distinct patterns of gene and
1349 protein expression elicited by organophosphorus pesticides in Caenorhabditis elegans.
1350 BMC Genomics. 2009;10: 202. doi:10.1186/1471-2164-10-202

1351 58. Helmcke KJ, Syversen T, Miller DM, Aschner M. Characterization of the effects of
1352 methylmercury on Caenorhabditis elegans. Toxicology and Applied Pharmacology.
1353 2009;240: 265–272. doi:10.1016/j.taap.2009.03.013

1354 59. Eom H-J, Kim H, Kim B-M, Chon T-S, Choi J. Integrative Assessment of Benzene
1355 Exposure to Caenorhabditis elegans Using Computational Behavior and Toxicogenomic
1356 Analyses. Environ Sci Technol. 2014;48: 8143–8151. doi:10.1021/es500608e

1357 60. Menzel R, Menzel S, Swain S, Pietsch K, Tiedt S, Witczak J, et al. The Nematode
1358 Caenorhabditis elegans, Stress and Aging: Identifying the Complex Interplay of Genetic
1359 Pathways Following the Treatment with Humic Substances. Frontiers in Genetics. 2012;3.
1360 Available: https://www.frontiersin.org/article/10.3389/fgene.2012.00050

1361 61. Trzebny A, Slodkowicz-Kowalska A, Becnel JJ, Sanscrainte N, Dabert M. A new method
1362 of metabarcoding Microsporidia and their hosts reveals high levels of microsporidian
1363 infections in mosquitoes (Culicidae). Molecular Ecology Resources. 2020;20: 1486–1504.
1364 doi:https://doi.org/10.1111/1755-0998.13205

1365 62. Lange B, Kaufmann AP, Ebert D. Genetic, ecological and geographic covariables
1366 explaining host range and specificity of a microsporidian parasite. Journal of Animal
1367 Ecology. 2015;84: 1711–1719. doi:10.1111/1365-2656.12421

1368 63. Bonneaud C, Tardy L, Giraudeau M, Hill GE, McGraw KJ, Wilson AJ. Evolution of both
1369 host resistance and tolerance to an emerging bacterial pathogen. Evolution Letters. 2019;3:
1370 544–554. doi:https://doi.org/10.1002/evl3.133

1371 64. Ayres JS, Schneider DS. Tolerance of Infections. Annual Review of Immunology. 2012;30:
1372 271–294. doi:10.1146/annurev-immunol-020711-075030

1373 65. Edgerton EB, McCrea AR, Berry CT, Kwok JY, Thompson LK, Watson B, et al.
1374 Activation of mosquito immunity blocks the development of transmission-stage filarial
1375 nematodes. PNAS. 2020;117: 3711–3717. doi:10.1073/pnas.1909369117

1376 66. Grover M, Fasseas MK, Essmann C, Liu K, Braendle C, Félix M-A, et al. Infection of C.
1377 elegans by Haptoglossa Species Reveals Shared Features in the Host Response to
1378 Oomycete Detection. Frontiers in Cellular and Infection Microbiology. 2021;11: 973.
1379 doi:10.3389/fcimb.2021.733094

1380 67. Osman GA, Fasseas MK, Koneru SL, Essmann CL, Kyrou K, Srinivasan MA, et al. Natural
1381 Infection of C. elegans by an Oomycete Reveals a New Pathogen-Specific Immune
1382 Response. Current Biology. 2018;28: 640-648.e5. doi:10.1016/j.cub.2018.01.029

1383 68. Lansdon P, Carlson M, Ackley BD. Wild-type Caenorhabditis elegans isolates exhibit
1384 distinct gene expression profiles in response to microbial infection. BMC Genomics.
1385 2022;23: 229. doi:10.1186/s12864-022-08455-2

1386 69. Wan YC, Troemel ER, Reinke AW. Conservation of Nematocida microsporidia gene
1387 expression and host response in Caenorhabditis nematodes. PLOS ONE. 2022;17:
1388 e0279103. doi:10.1371/journal.pone.0279103

1389 70. Dirksen P, Assié A, Zimmermann J, Zhang F, Tietje A-M, Marsh SA, et al. CeMbio - The
1390 Caenorhabditis elegans Microbiome Resource. G3: Genes, Genomes, Genetics. 2020;10:
1391 3025–3039. doi:10.1534/g3.120.401309

1392 71. Powell JR, Ausubel FM. Models of Caenorhabditis elegans Infection by Bacterial and
1393 Fungal Pathogens. In: Ewbank J, Vivier E, editors. Innate Immunity. Totowa, NJ: Humana
1394 Press; 2008. pp. 403–427. doi:10.1007/978-1-59745-570-1_24

1395 72. Norris AD, Kim H-M, Colaiácovo MP, Calarco JA. Efficient Genome Editing in
1396 Caenorhabditis elegans with a Toolkit of Dual-Marker Selection Cassettes. Genetics.
1397 2015;201: 449–458. doi:10.1534/genetics.115.180679

1398 73. Stiernagle T. Maintenance of C. elegans. WormBook. 2006; 1–11.
1399 doi:10.1895/wormbook.1.101.1

1400 74. Luallen RJ, Bakowski MA, Troemel ER. Characterization of Microsporidia-Induced
1401 Developmental Arrest and a Transmembrane Leucine-Rich Repeat Protein in
1402 Caenorhabditis elegans. PLOS ONE. 2015;10: e0124065.
1403 doi:10.1371/journal.pone.0124065

1404 75. Willis AR, Jarkass HTE, Reinke AW. Studying Inherited Immunity in a Caenorhabditis
1405 elegans Model of Microsporidia Infection. JoVE (Journal of Visualized Experiments).
1406 2022; e63636. doi:10.3791/63636

1407 76. Schindelin J, Arganda-Carreras I, Frise E, Kaynig V, Longair M, Pietzsch T, et al. Fiji: an
1408 open-source platform for biological-image analysis. Nature Methods. 2012;9: 676–682.
1409 doi:10.1038/nmeth.2019

1410 77. Langmead B, Salzberg SL. Fast gapped-read alignment with Bowtie 2. Nat Methods.
1411 2012;9: 357–359. doi:10.1038/nmeth.1923

1412 78. Li H, Handsaker B, Wysoker A, Fennell T, Ruan J, Homer N, et al. The Sequence
1413 Alignment/Map format and SAMtools. Bioinformatics. 2009;25: 2078–2079.
1414 doi:10.1093/bioinformatics/btp352

1415 79. Garrison E, Marth G. Haplotype-based variant detection from short-read sequencing. 2012
1416 [cited 4 Jun 2022]. doi:10.48550/ARXIV.1207.3907

1417 80. Cook DE, Andersen EC. VCF-kit: Assorted utilities for the variant call format.
1418 Bioinformatics. 2017; btx011. doi:10.1093/bioinformatics/btx011

1419 81. Wang L, Wang S, Li W. RSeQC: quality control of RNA-seq experiments. Bioinformatics.
1420 2012;28: 2184–2185. doi:10.1093/bioinformatics/bts356

1421 82. Ewels P, Magnusson M, Lundin S, Käller M. MultiQC: summarize analysis results for
1422 multiple tools and samples in a single report. Bioinformatics. 2016;32: 3047–3048.
1423 doi:10.1093/bioinformatics/btw354

1424 83. Bray NL, Pimentel H, Melsted P, Pachter L. Near-optimal probabilistic RNA-seq
1425 quantification. Nat Biotechnol. 2016;34: 525–527. doi:10.1038/nbt.3519

1426 84. Marini F, Binder H. pcaExplorer: an R/Bioconductor package for interacting with RNA-seq
1427 principal components. BMC Bioinformatics. 2019;20: 331. doi:10.1186/s12859-019-2879-1

1428 85. Chen K, Franz CJ, Jiang H, Jiang Y, Wang D. An evolutionarily conserved transcriptional
1429 response to viral infection in Caenorhabditis nematodes. BMC Genomics. 2017;18: 303.
1430 doi:10.1186/s12864-017-3689-3

1431 86. Eddy SR. Accelerated Profile HMM Searches. PLOS Computational Biology. 2011;7:
1432 e1002195. doi:10.1371/journal.pcbi.1002195

1433 87. Kuleshov MV, Jones MR, Rouillard AD, Fernandez NF, Duan Q, Wang Z, et al. Enrichr: a
1434 comprehensive gene set enrichment analysis web server 2016 update. Nucleic Acids Res.
1435 2016;44: W90–W97. doi:10.1093/nar/gkw377

1436